Title

Top-down acetylcholine enables social discrimination via unlocking action potential generation in olfactory bulb vasopressin cells

Authors

Hajime Suyama, Veronica Egger, Michael Lukas

Institute of Zoology, Neurophysiology, University of Regensburg, 93040 Regensburg, Germany

Corresponding author

Michael Lukas

Institute of Zoology, Neurophysiology, University of Regensburg, 93040 Regensburg, Germany

e-mail: michael.lukas@ur.de

Abstract

Social discrimination in rats requires activation of the intrinsic bulbar vasopressin system, but it is unclear how this system comes into operation. Here we show that a higher number of bulbar vasopressin cells (VPC) is activated by stimulation with a conspecific compared to rat urine, indicating that VPC activation depends on more than olfactory cues during social interaction. *In-vitro* slice electrophysiology combined with pharmacology and immunohistochemistry then demonstrated that centrifugal cholinergic inputs from the diagonal band of Broca can enable olfactory nerve-evoked action potentials in VPCs via muscarinic neuromodulation. Finally, such muscarinic activation of the vasopressin system is essential for vasopressin-dependent social discrimination, since recognition of a known rat could be blocked by a muscarinic antagonist and rescued by additional application of vasopressin. For the first time, we demonstrated that top-down cholinergic modulation of bulbar VPC activity in a social context is crucial for individual social discrimination in rats.

Introduction

Many mammals use olfactory cues as a fundamental communication tool, in particular for the recognition and discrimination of individual conspecifics. A prominent example for a behavioral reaction that depends on olfaction-based discrimination of individuals is that ewes recognize the body odor of their own offspring and as a result, deny strange lambs to suckle [1]. Moreover, in prairie voles, the olfaction-based recognition of their mating partners enables them to establish monogamous pairbonds [2]. Rats and mice, the most common mammalian laboratory animals, also discriminate individual conspecifics via their odor signatures. This discrimination can then lead to various essential behavioral reactions [3]. To quantify the ability of rats to recognize individual odor signatures, so-called social discrimination tests are used [4]. Briefly, rats are exposed to a conspecific (sampling phase). After a short time of separation, rats are exposed to the same and a novel conspecific (discrimination phase). If the rats recognize the known conspecific, they investigate it less compared to the novel conspecific [4]. However, whether and

how non-olfactory cues are involved in this paradigm are still unclear.

The peptidergic neuromodulator vasopressin (VP), an important mediator of various social behaviors in the mammalian brain [5], is a major player in facilitating social discrimination. For example, microinjection of VP into the OB enhances social discrimination [6]. Further, Tobin et al. [7] demonstrated the existence of an intrinsic bulbar VP system, consisting of VP-expressing cells (VPCs) and an impairment of social discrimination by the blockade of bulbar V1a receptors.

Recently, we classified these bulbar VPCs as non-bursting superficial tufted cells [8]. The apical dendrite of a VPC innervates a single OB glomerulus with a dense tuft, suggesting that VPCs receive excitatory inputs from the olfactory nerve (ON) just like other bulbar cells with glomerular tufts such as mitral cells (MCs) [9], e.g. during sampling of conspecific's body odors. Intriguingly, we found that electric ON stimulation does not excite VPCs but elicits primarily inhibitory postsynaptic potentials (IPSPs) as recorded at the soma. This dominant GABAergic input masks a delayed barrage of excitatory postsynaptic potentials (EPSPs). Therefore, if olfactory input inhibits VPCs and thus cannot trigger VP release, it is still unclear how intrinsic VP neurotransmission is possible during social discrimination. We hypothesize that in order to excite VPCs and allow VP release, non-ON inputs are required that either inhibit the GABAergic origin of the ON-evoked inhibition and/or deliver enough direct excitation onto VPCs to outweigh the inhibition.

Naturally, during social interaction, rats sample not only olfactory cues, but also other sensory cues, like vocalizations or touch [10, 11]. Thus, we suggest that the perception of non-olfactory cues during social interaction may be required for olfactory activation of bulbar VPCs. For integration of non-olfactory social cues into bulbar neurotransmission, top-down modulation is the most likely option. The most prominent modulatory centrifugal inputs to the OB are noradrenergic, serotonergic, and cholinergic fibers [12-14]. Those neuromodulatory systems were shown to be involved in changes of internal states [15-17], but more interestingly they are also facilitators of social discrimination behavior, acting either directly in the OB or other brain regions [18-20]. Thus, we propose them as candidate activators of the bulbar VP system.

This leads to the following questions: (1) Are bulbar VPCs activated during social interactions, and which stimuli (i.e. social odor alone or multisensory social interaction) activate them? (2) Can

the candidate centrifugal neuromodulators increase excitation of bulbar VPCs? (3) If so, is centrifugal modulation of bulbar VPCs essential for VP-dependent social discrimination? We approach these questions by investigating neuronal activity and synaptic mechanisms *in-vitro* as well as applying behavioral pharmacology *in-vivo*.

Results

Social interaction activates bulbar VPCs

As we recently demonstrated [8] that ON stimulation alone primarily inhibits VPCs, we suggest that (1) olfactory social cues alone are insufficient to excite VPCs and (2) VPC excitation is driven or unlocked by non-olfactory, top-down social signals. To test this hypothesis, we chose urine as an isolated olfactory social cue [21] and a novel male juvenile rat as a complete social stimulus. Thus, juvenile VP-eGFP male rats [22] were exposed to either, water (control), rat urine, or a novel juvenile rat and we compared the neuronal activity of bulbar VPCs between these different types of stimulation as reflected in phosphorylated extracellular signal-regulated kinase (pERK) induction in eGFP-labeled VPCs (Fig. 1A). The total number of eGFP$^+$ VPCs was not different across animal groups (Fig. 1B; p=0.670, water n=10, urine n=9, rat n=10)$_a$. Indeed, the exposure to a rat resulted in a significantly higher number of pERK$^+$ VPCs than the exposure to water or urine (Fig. 1C; rat vs. water p=0.02, rat vs. urine p=0.047, water vs. urine p=0.204)$_b$. This finding indicates that additional social-stimulus specific inputs beyond the olfactory cues in urine are necessary for the activation of VPCs. Also, the number of pERK$^+$ MCs was increased in the same set of animals following the exposure to a rat compared to water or urine (Fig. 1D; rat vs. water p=0.025, rat vs. urine p=0.034, water vs. urine p=0.949)$_c$.

In addition, we analyzed activation of VPCs and mitral/tufted cells (M/TCs) in the accessory olfactory bulb (AOB), as the main olfactory bulb (MOB) and the AOB are related with social memory in rats [23]. However, pERK$^+$ VPCs were rarely observed (Supplemental Fig. 1C; water 0.4 ± 0.1 VPCs (2.1 ± 0.7 %), urine 0.5 ± 0.1 VPCs (2.4 ± 0.8 %), rat 1.0 ± 0.2 VPCs (3.4 ± 0.8 %)), although VPC activation in the rat exposure group was significantly higher than in the water or urine exposure group (rat vs. water p=0.019, rat vs. urine p=0.033, water vs. urine

p=0.804, n=9)[e]. Thus, AOB VPCs are unlikely to play an important role in facilitating social discrimination compared to MOB VPCs. The number of activated AOB M/TCs was not different between groups (Supplemental Fig. 1D; p=0.164)[f].

Taken together, more VPCs were activated by social interaction than by investigating urine, and MOB VPCs showed more prominent activation than AOB VPCs. Thus, additional stimuli might be needed to specifically activate VPCs via modulation, i.e. disinhibition or increasing excitation.

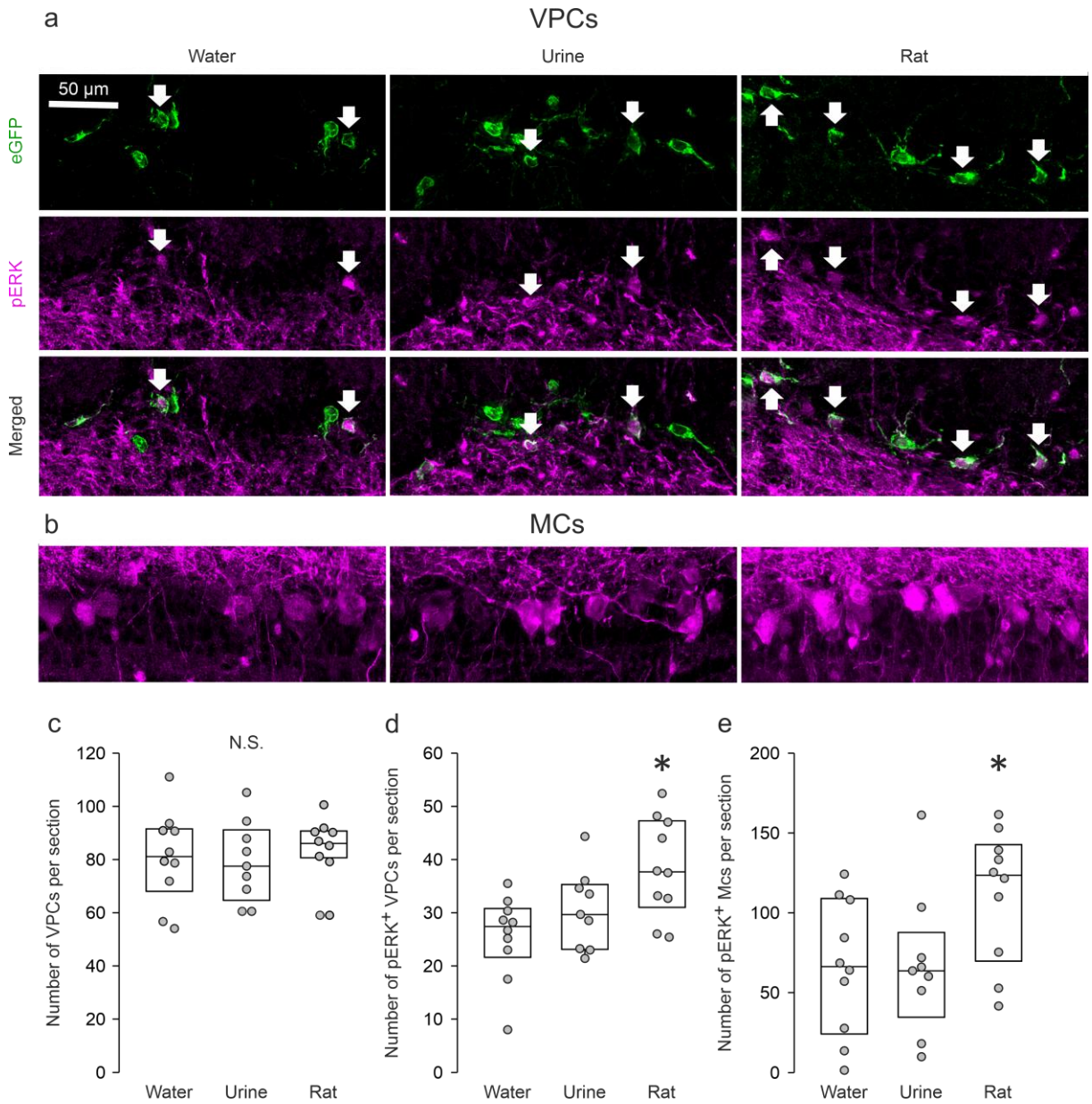

Fig. 1 **Social interaction activates bulbar VPCs**

(a+b) Representative average z-projections of the olfactory bulb that were immune-stained for eGFP (green, CF488) and pERK (magenta, CF 594). (a) VPCs. Arrows indicate cells that are double-labeled for eGFP and pERK. (b) pERK$^+$ MCs. (c-e) Number of VPCs, of pERK$^+$ VPCs or of pERK$^+$ MCs per section in different stimulation groups. Data are presented as box-plots including median and distribution of single data points. ANOVA, LSD single comparison, * $p<0.05$ vs. Water or Urine, n=10 (water), n=9 (urine), n=10 (rat). Scale bar, 50 µm.

Cholinergic modulation triggers excitatory responses and action potentials during ON stimulation of VPCs

The OB, especially the glomerular layer (GL) and the external plexiform layer (EPL) where VPCs are located, receives many centrifugal projections that release catecholaminic neuromodulators. These projections originate from various brain areas [12-14]. The receptors of these neuromodulators are expressed in the entire MOB [24, 25]. Our hypothesis was that such centrifugal neuromodulatory inputs to the MOB mediate social-stimulus specific modulation of VPC activity. To examine such centrifugal neuromodulator effects, we performed whole-cell patch-clamp recordings from VPCs and stimulated the ON [8] while bath-applying neuromodulators (Fig. 2a). The doses used were chosen based on minimal doses reported to elicit *in-vitro* effects [26-28].

5-HT (20 µM) decreased the amplitudes of ON-evoked IPSPs to 69.7 ± 10.1 % of control (Fig. 2B and C; p=0.012, n=8 from 8 rats)$_g$. NA (20 µM) reduced IPSP amplitudes to 62.9 ± 9.5 % of control (Fig. 2D and E; p=0.011, n=9 from 8 rats)$_h$. However, inhibition was not relieved entirely in any of these experiments. Thus, 5-HT and NA modulation can reduce ON-evoked inhibition of VPCs, but are unlikely to enable activation of VPCs as observed during social interaction (Fig. 1).

In contrast, wash-in of ACh (100 µM) switched inhibitory to excitatory responses in the majority of VPCs: 65 % of VPCs fired action potentials (APs, 13 out of 20 cells from 19 rats), and 10 % of VPCs responded with EPSPs to ON stimulation (Fig. 2F and G). The amplitudes of PSPs were significantly increased during ACh application versus control (Fig. 2G; p<0.001)$_i$. Accordingly, the distribution of response amplitudes in the presence of ACh was significantly different from control (Fig. 2H; p<0.001)$_j$, as well as different from the 5-HT or NA condition (Fig. 2I; ACh vs. 5-HT p=0.003, ACh vs. NA p=0.002, 5-HT vs. NA p=1.0)$_k$. Although evoked APs or EPSPs were observed, ACh did not increase intrinsic excitability in VPCs as there were no differences in spiking rates of AP trains during somatic current injections (Supplemental Fig. 2A; Treatment p=0.417, Current intensity p<0.001, Treatment*Current intensity p=0.528, n=10 from 9 rats)$_l$. Also, increased latency of the first spike was observed with lower current indicating rather lower excitability during ACh treatment (Supplemental Fig. 2B; Treatment p=0.080, Current intensity

$p<0.001$, Treatment*Current intensity $p=0.015$, ACh vs. ACSF (40 pA) $p=0.029)_m$.

In addition to these top-down catecholaminic neuomodulatory inputs, rat AOB M/TCs send axons to the dorsal MOB that potentially result in interaction between the AOB and the MOB [29]. Also, it was shown that pheromonal AOB inputs are involved in social discrimination [23, 30]. To investigate if these AOB inputs can elicit excitation in MOB VPCs, we electrically stimulated the AOB during whole-cell patch-clamp recordings from MOB VPCs. Acute *in-vitro* slices for these experiments were prepared at a cutting angle that should preserve the respective projections [29] (Supplemental Fig. 2C). However, no VPC showed any responses (Supplemental Fig. 2D; n=21), suggesting that modulation of MOB VPCs via AOB inputs is unlikely.

Taken together, we have identified ACh as a strong candidate neuromodulator that unlocks VPC APs that would allow for axonal VP release.

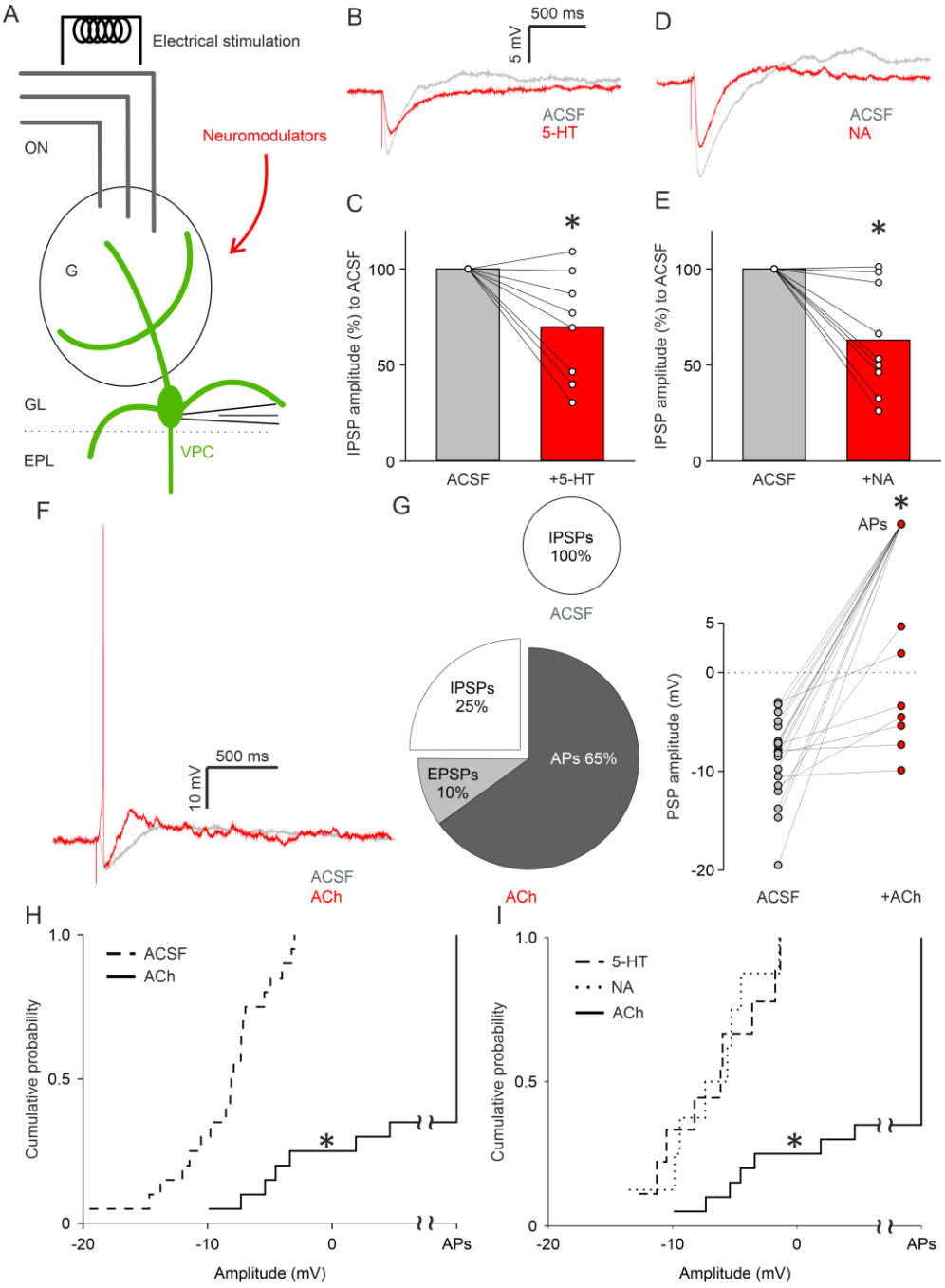

Fig. 2 **Cholinergic modulation triggers excitatory responses and action potentials during ON stimulation of VPCs**
(A) Schematic drawing of the experimental setup. Whole-cell patch-clamp recordings in 300 µm *in- vitro* slices of response from VPCs to electrical ON stimulation (50 µA, 100 µs, 30 s intervals) (B+D) Representative averaged traces of responses following ON stimulation in the ACSF condition (artificial cerebrospinal fluid, black) and during bath application of 5-HT (20 µM) and NA (noradrenaline 20 µM, red). (C+E) Cumulative analysis of normalized IPSP amplitudes of evoked IPSPs to the ACSF control condition during bath application of 5-HT (n=8) and NA (n=9). Data are presented as means including distribution of single data points. Lines between data points represent related measurements. Related-Samples Wilcoxon Signed Rank Test, *p<0.05. (F) Representative averaged traces of responses to ON stimulation in the ACSF condition (black) and a single trace during bath application of ACh showing APs (acetylcholine, red). (G) (left) Pie-charts represent the proportion of VPCs showing either APs, EPSPs or IPSPs in the ACSF and ACh condition. (right) Cumulative analysis of amplitudes of PSPs or APs (set as 100 mV) in the ACSF and ACh condition. Related-Samples Wilcoxon Signed Rank Test, *p<0.05. n=20. (H+I) Cumulative probability of evoked PSP amplitudes in the ACSF, 5-HT, NA or ACh condition (n=20/8/9/20). The amplitudes of APs were set as 100 mV. Kruskal-Wallis test for variation comparison, Bonferroni, *p<0.05 ACh vs. ACSF, 5-HT, NA.
ON, olfactory nerve. G, glomerulus. GL, glomerular layer. EPL, external plexiform layer. VPC, vasopressin cell.

ACh modulates both ON-evoked inhibition and excitation via muscarinic receptors but does not increase intracellular Ca^{2+} influx

To further dissect the cellular underpinnings of these ACh effects, we quantified the amplitude changes of evoked IPSPs in VPCs that did not turn into APs or EPSPs in ACh (5 out of 20 cells). In these cells, ACh decreased the amplitudes of evoked IPSPs to 67.8 ± 11.3 % of control (Fig. 3A and B; p=0.043, n=5 from 5 rats)$_n$. This observation indicates that ACh, like 5-HT and NA, also reduces inhibition of VPCs. As there were also obvious excitatory modulatory effects of ACh as VPCs showed APs or EPSPs (Fig. 2F and G), we examined the excitatory components of ON-driven inputs in VPCs. After the detection of evoked IPSPs in ACSF, bicuculline, a GABA-A receptor antagonist, was applied to unmask evoked EPSPs [8], followed by ACh administration to examine whether ACh acts via increasing the amplitudes of these EPSPs. First of all, we observed slower onsets of bicuculline-unmasked EPSPs than of evoked APs during ACh application alone (latency of EPSPs 32.8 ± 12.1 ms (n=6 from 5 rats), APs 8.6 ± 0.7 ms (n=13 from 13 rats), p=0.002)$_o$. Half of the VPCs showed occasionally evoked APs under ACh application (Fig. 3D; 3 out of 6 cells from 5 rats). We collected all traces without APs to measure the amplitudes of EPSPs. ACh application increased the amplitudes of evoked EPSPs to 204.4 ± 39.8 % from bicuculline alone (Fig. 3D; p=0.043, n=5 from 5 rats)$_p$. This increase in EPSP amplitudes indicates that ACh enhances ON-evoked excitation to activate VPCs, on top of disinhibition, possibly via acting on both excitatory and inhibitory glomerular neurons [31, 32].

Since VPCs innervate glomeruli via apical dendritic tufts [8], ACh-mediated excitation may happen already at the tuft. To investigate subcellular excitation in VPCs, we simultaneously performed whole-cell patch-clamp recordings of PSPs from the soma and imaged intracellular Ca^{2+} changes in the tufts and near the soma during ON stimulation using two-photon microscopy (Fig. 3E and F). A single ON stimulation was able to elicit Ca^{2+} influx in the tufts but not at the soma of VPCs (Fig. 3F and G; tuft vs. soma p=0.002, n=8 from 8 rats)$_q$. The finding of a distal postsynaptic Ca^{2+} entry that cannot be detected near the soma, is consistent with the concurrent observation of strong GABAergic inhibition at the soma suggesting that excitation at the tufts is inhibited alongside the apical dendrite. Upon ACh wash-in, although APs and EPSPs were

recorded at the soma, ACh did not further increase Ca^{2+} influx neither in the tufts or the soma (treatment p=0.203)$_q$. This observation implies that excitation in the tuft is not sensitive to ACh and not responsible for the unlocking of somatic APs.

To narrow down candidate input pathways responsible for ACh effects on VPCs, we next focused on ACh receptor subtypes. We used mecamylamine (20 μM) and atropine (10 μM) to antagonize nicotinic and muscarinic ACh receptors, respectively. We measured evoked IPSPs before and during antagonist administration and subsequently added ACh (100 μM). Administration of antagonists alone showed no effects on evoked IPSPs, as all cells showed IPSPs (Fig. 3H-K; mecamylamine n=11 from 9 rats, atropine n=7 from 4 rats) and their amplitudes were similar to the ACSF condition (Fig. 3I and K; ACSF vs. mecamylamine p=1.0, atropine p=0.156)$_{r,s}$. 18 % and 9 % of cells under mecamylamine-ACh application showed evoked APs and EPSPs, respectively (Fig. 3I). The amplitudes of evoked IPSPs (73 %), however, were significantly smaller in the mecamylamine-ACh condition than in mecamylamine application alone (Fig. 3H and I; p=0.024, n=8 from 7 rats)$_r$. Thus, blockade of nicotinic receptors could not fully suppress ACh-mediated excitatory effects, whereas all cells in the atropine-ACh condition were still inhibited by ON stimulation (Fig. 3K), with similar IPSP amplitudes between atropine and atropine-ACh conditions (Fig. 3J and K; p=0.156)$_s$. These results indicate that the muscarinic pathway is the major player in both increasing excitation and disinhibition of ON-stimulated VPCs.

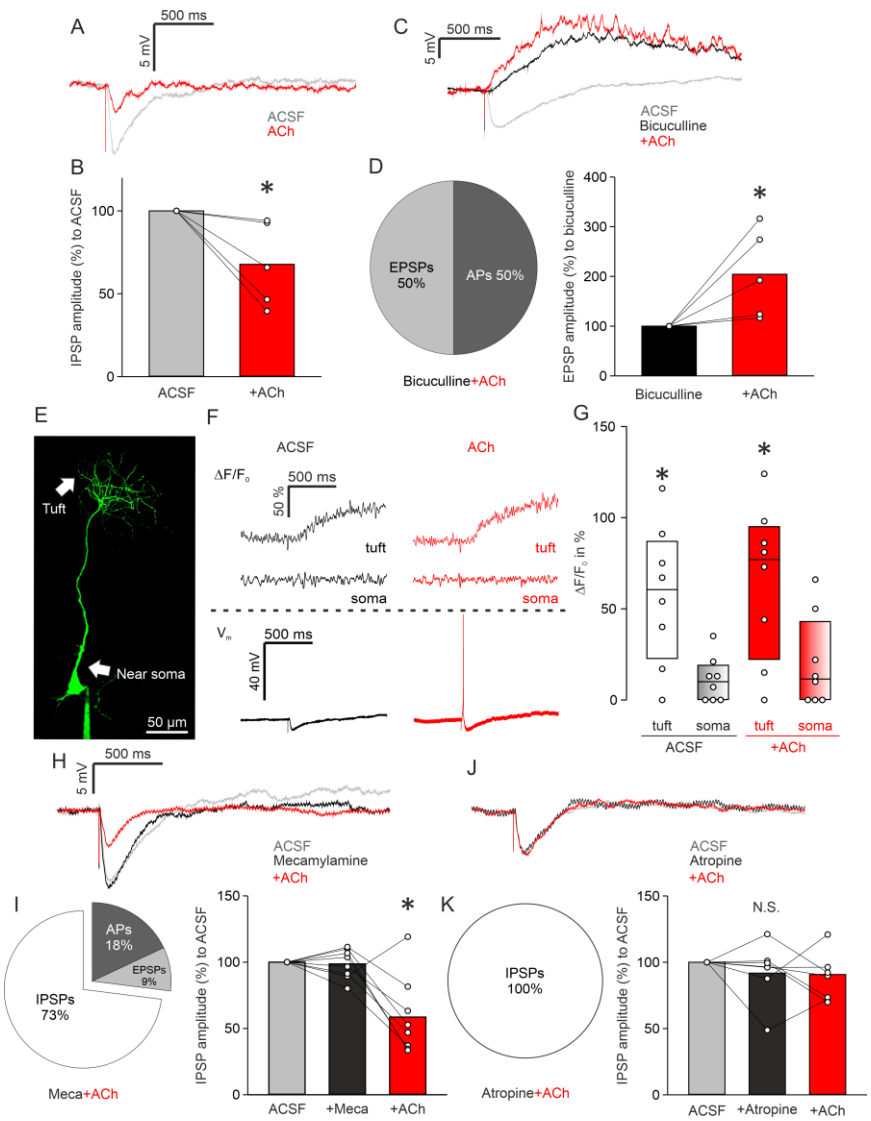

Fig. 3 **ACh modulates both ON-evoked inhibition and excitation via muscarinic receptors but does not increase intracellular Ca^{2+} influx**

Whole-cell patch-clamp recordings in 300 µm *in vitro* slices of response from VPCs to electrical ON stimulation (50 µA, 100 µs, 30 s intervals). (A) Representative averaged traces of responses following ON stimulation in the ACSF condition (grey) and during bath application of ACh (acetylcholine, red) showing reduced IPSPs. (B) Cumulative analysis of normalized evoked IPSP amplitudes to the ACSF condition during bath application of ACh (n=5). (C) Representative averaged traces of responses following ON stimulation in the ACSF condition (grey) and during bath application of bicuculline (50 µM, black) and additional application of ACh (100 µM, red). (D) (left) Pie-chart representing the proportion of cells showing either APs or EPSPs in the ACh condition (n=6). (right) Cumulative analysis of normalized evoked EPSP amplitudes to the bicuculline condition during additional application of ACh (n=5). (B+D) Related-Samples Wilcoxon Signed Rank Test, *p<0.05 vs. ACSF/bicuculline. (E) Representative picture of the VPC filled with OGB-1. Arrows indicate the tuft and the soma. Scale bar, 50 µm. (F) (top) Representative averaged traces of Ca^{2+} influx in the tuft and the soma. (bottom) Representative averaged traces of responses following ON stimulation (ACSF, black; ACh, red). (G) $\Delta F/F_0$ in % from baseline. Data are presented as box-plots including median and distribution of single data points. (2) × (2) mixed model ANOVA (location [within subject] × treatment [within-subject]), *p<0.05 vs. soma whithin the condition. n=8. (H+J) Representative averaged traces of responses following ON stimulation in the ACSF condition (grey) and during bath application of mecamylamine/atropine (20 µM/10 µM, black), and additional application of ACh (100 µM, red). (J+K) (left) Pie-chart representing the proportion of cells showing either APs, EPSPs or IPSPs in the +ACh condition. n=11/7. (right) Cumulative analysis of normalized evoked IPSP amplitudes to the mecamylamine/atropine condition during additional bath application of ACh (n=8/7). Friedman test, Dunn for single comparisons, *p<0.05 vs. Meca (mecamylamine). N.S., not significant.

Cholinergic cells in the HDB are activated during social interaction

Our results reveal that ACh can flip ON-evoked inhibition of bulbar VPCs into excitation *in-vitro*. If this activating drive of ACh is indeed involved in triggering VPC excitation in behaving rats, we hypothesized that ACh is likely released into the OB during social interaction. In other words, ACh neurons that are known to project to the OB from the horizontal limb of the diagonal band of Broca (HDB) [33, 34] should get activated in a social context. Activity of the cholinergic system is correlated with changes in sensations or internal states such as arousal or attention [35-40]. Moreover, it was shown that stimulation of HDB ACh neurons can sharpen the odor responses of MOB M/TCs [41, 42]. Since we had obtained whole brains from the exposure experiments (water, rat urine, conspecific), we next investigated the activity of ACh neurons in the HDB. To visualize activated HDB neurons and specifically activated ACh neurons, we stained the HDB against pERK and choline acetyltransferase (ChAT) (Fig. 4A). The total number of $pERK^+$ HDB cells was not significantly different between all groups (Fig. 4B; p=0.104, water n=5, urine n=5, rat n=6)$_t$. However, the number of $pERK^+$ ACh neurons in the rat exposure group was significantly higher than that in the urine exposure group (Fig. 4C; p=0.011)$_u$. The results indicate that more HDB ACh neurons are activated by social interactions than by investigating social odor stimuli alone and thus also more likely to excite VPCs specifically during social interactions.

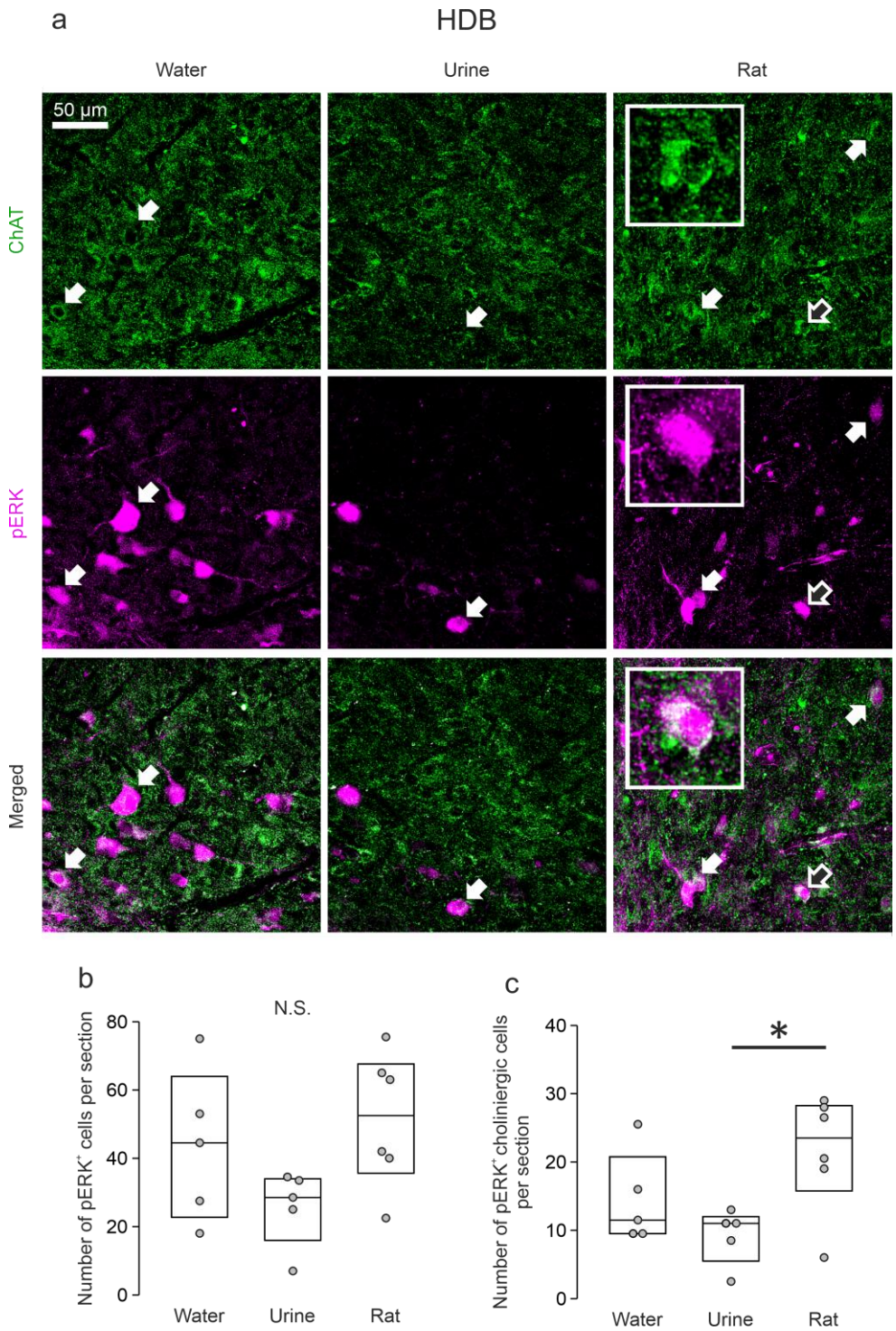

Fig. 4 **Cholinergic cells in the HDB are activated during social interaction**

(a) Representative average z-projections of the HDB (horizontal limb of the diagonal band of Broca) that were immune-stained for ChAT (choline-acetyltransferase, green, CF488) and pERK (magenta, CF 594). Arrows indicate cells that are double-labeled for pERK and ChAT. Insets show enlarged pictures of the cell indicated by blank arrows. Scale bar, 50 µm. (b+c) Number of $pERK^+$ cells or $pERK^+$ cholinergic cells per slice in different experimental groups. Data are presented as box-plots including median and distribution of single data points. ANOVA, LSD for single comparisons, *p<0.05 Rat vs. Urine, n=5 (water), n=5 (urine), n=6 (rat).

Atropine-induced impairment of social discrimination is rescued by VP microinjection into the OB in male rats

Our data so far demonstrated an excitatory effect of bulbar ACh on ON-evoked VPC activity via muscarinic receptors as well as the activation of both systems, intrinsic bulbar VP and HDB ACh, during social interaction. These observations are in line with behavioral studies that demonstrate that pharmacological blockade of bulbar V1a receptor or systemic ACh activity diminishes social discrimination abilities in rats [7, 43]. To examine if the cellular mechanisms we found in the OB indeed play a role for social discrimination in behaving rats, we tested if blockade of muscarinic ACh signaling in the OB impairs social discrimination and if a later additional VP injection, mimicking potential ACh-facilitated VP release, could rescue a possibly impaired behavior. Thus, we performed microinjections of atropine (1 µg/ 1 µL per hemisphere) or vehicle (ACSF, 1 µL per hemisphere) followed by either VP (1 ng/ 1 µL per hemisphere) or vehicle before the sampling phase of a social discrimination test (Fig. 5a). In this test, the ability to discriminate two individuals is measured in terms of how long rats spend time for investigating a novel versus a known stimulus rat.

Control rats that received only vehicle investigated the novel stimulus rat significantly more than the known rat, indicating intact social discrimination (Fig. 5D; $p=0.033$, $n=13)_v$. In contrast, atropine-injected rats showed a similar duration of investigation towards both novel and known stimulus rats (Fig. 5E; $p=0.240$, $n=14)_w$. Thus, the blockade of muscarinic signaling in the OB indeed impaired social discrimination. This effect is most likely caused by a disruption of the activation of the bulbar VP system and thus a potential reduction of bulbar VP release during social interaction, because atropine-VP injected rats significantly preferred investigating the novel stimulus rat over the known one (Fig. 5F; $p=0.031$, $n=14)_x$. Therefore, their ability to discriminate a known from a novel stimulus was rescued by additional VP injection.

This final experiment thereby supports our hypothesis based on our findings *in-vitro* that the activity of the bulbar VP system that is essential for the discrimination of social odor signatures is triggered by centrifugal ACh inputs during social interaction.

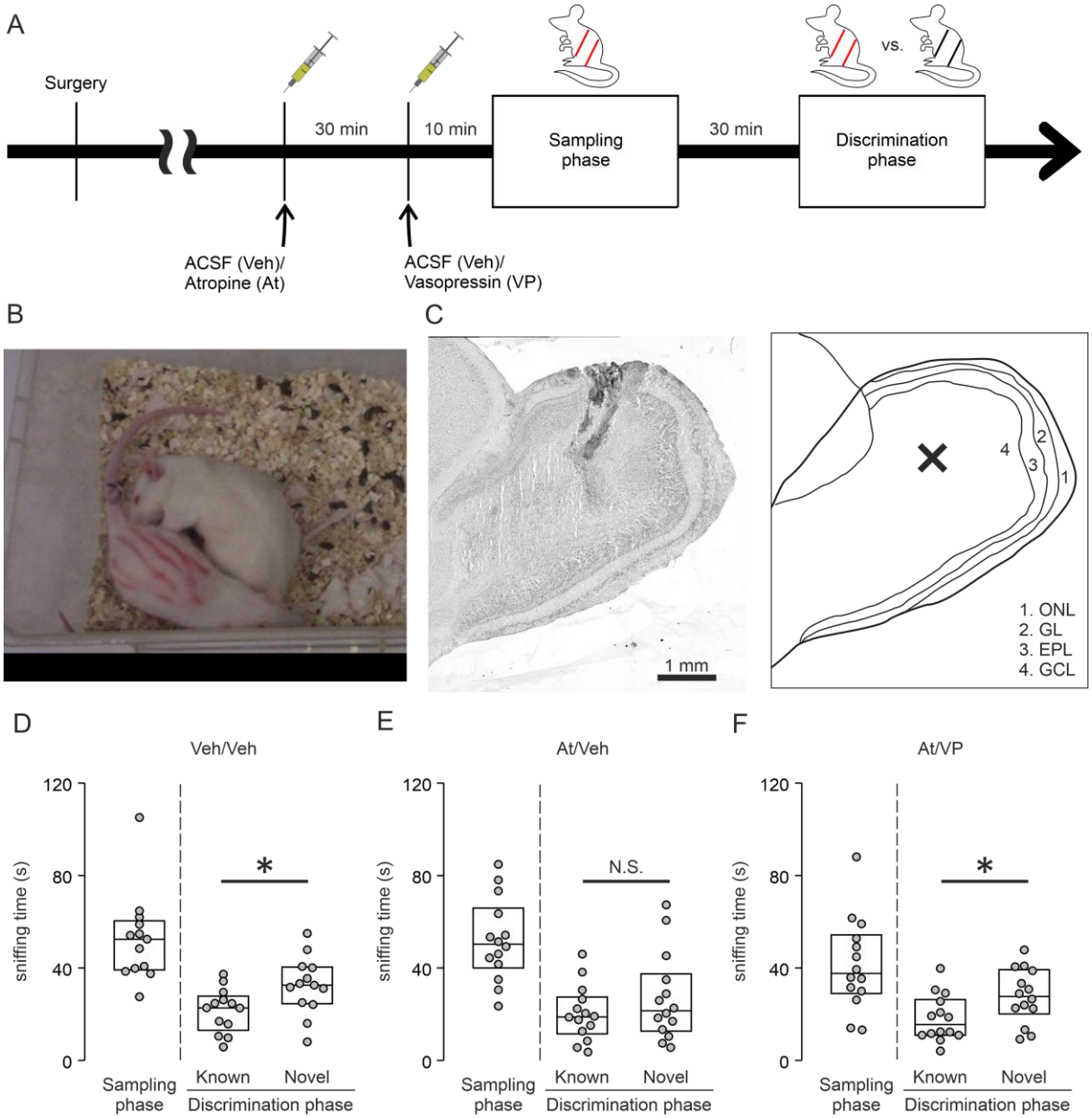

Fig. 5 **VP microinjection into the OB rescues the atropine-induced impairment of social discrimination in male rats**
(A) Schematic time course of the experimental design. (B) Rat (5 weeks) without markings representing anogenital sniffing toward a stimulus rat (3 weeks) with red markings. (C) (left) Representative picture of the OB with dye injection via injection system, counterstained with Cresyl violet. (right) Schematic picture of the olfactory bulb. The cross indicates the approximate injection position in the left picture. ONL, olfactory nerve layer; GL, glomerular layer; EPL, external plexiform layer; GCL, granule cell layer. (D-F) Amount of time (s) that rats investigate stimulus rats in the sampling phase and in the discrimination phase (known or novel rat) following microinjection (1 µL per bulb) with only vehicle (D), atropine (1 µg/ 1 µL) and vehicle (E) or atropine and VP (1 ng/ 1 µL, F). Data are presented as box-plots including median and distribution of single data points. Paired Samples t-Test between known and novel, *p<0.05, n=13 (Veh/Veh), n=14 (At/Veh), n=14 (At/VP).

Discussion

Is bulbar VPC activity triggered specifically during social interaction?

Social discrimination in rats depends on the presence of endogenous VP in the OB [7], which implies that social interaction can trigger VP release, via the activation of bulbar VPCs. Indeed, we observed increased levels of bulbar VPC activation during social interaction with a juvenile rat, using pERK (Fig. 1D). pERK itself can immediately increase neuronal excitability via suppressing transient K^+ channel activity in hippocampal CA1 pyramidal cells [44] and enhancing AMPA and NMDA receptor activity in neurons of the spinal cord [45]. Both findings imply excitatory functions of pERK activation in neurons. Thus, our results suggest that in the context of social interaction, VPC activity, hence the probability of bulbar VP release, is substantially higher than during investigating odors without the additional context of social interaction. Intriguingly, this is apparently at variance with the findings from Wacker et al. [46], who reported that social interaction cannot trigger the expression of the immediate early genes c-Fos or Egr-1 in bulbar VPCs. However, as discussed by them, a missing expression signal of those genes might be explained by their general absence of expression in bulbar VPCs. Since we know that VPCs are primarily inhibited by ON inputs *in-vitro* [8], we hypothesized that additional inputs from outside of the OB are responsible for the activation of VPCs, involving the transmission of a social context during social interaction.

Can Pheromones modulate bulbar VPCs during social odor perception?

Pheromones from conspecifics are detected by rodents during social interactions and were shown to directly influence social behaviors, such as sexual behavior or aggression between conspecifics [47, 48]. Thus, pheromones would be an obvious way to deliver social context via social interactions. Indeed, M/TCs in the AOB, the first pheromonal relay station in the brain, are known to innervate the dorsal MOB and therewith could also excite bulbar VPCs [29]. In our hands, electric stimulation of the AOB failed to elicit any excitatory responses in MOB VPCs in *in-vitro* sagittal slice experiments (Supplemental Fig. 2C, D). Thus, it seems rather unlikely that

pheromones alone can directly trigger excitatory synaptic responses in MOB VPCs. Moreover, although social interaction increases c-Fos expression in the AOB not differentiating M/TCs and GCs [30], we did not find any differences in the number of pERK$^+$ AOB M/TCs between the rat, urine, and control water exposure group (Supplemental fig. 1C, D). Also, we rarely observed pERK$^+$ VPCs in the AOB itself, neither following urine exposure nor social interaction (only 1 or even less cells on average per slice). Noack et al. [30] showed that a stream of room air can already increase c-Fos expression in AOB M/TCs and GCs. Thus, we cannot exclude that non-specific activity-induced pERK possibly masks stimulus-specific activation of AOB M/TCs. However, both low levels of pERK activation in the AOB VPCs during social interaction and the apparent lack of connectivity between AOB input and MOB VPCs indicate that pheromonal AOB signaling is not the prominent trigger for VP-dependent individual social discrimination in the MOB. Also, while removal of the vomeronasal organ initially prevents social recognition of same sex individuals, it is reinstated after 14 days, indicating that AOB functioning is not required for social recognition *per se* [23]. Nevertheless, the AOB is crucial for individual discrimination in the context of reproduction. For example, the pheromonal memory of the stud male in female mice results in a pregnancy block induced by odors of male strangers. This consequence of social odor recognition, known as the Bruce effect, depends on pheromonal processing in the AOB [49]. This indicates that the AOB may be essential for individual discrimination in certain situations, such as in a reproductive context, but not necessarily in social discrimination in general.

How does ACh modulate VPC activity?

Cholinergic neurons in the HDB are known to provide centrifugal neuromodulatory inputs to the GL of the OB, where VPCs are predominantly located [8, 33, 34]. Following social interaction, the number of pERK$^+$ cholinergic HDB neurons was significantly higher compared to rat urine exposure alone (Fig. 4C) indicating that cholinergic activation might be involved in bulbar VPC activation in the rat exposure group (Fig. 1C). Accordingly, we observed that ON-evoked IPSPs are reversed into EPSPs/APs in 75 % of examined VPCs during ACh administration *in-vitro* (Fig. 2G). Moreover, we showed that ACh induces both, disinhibition and stronger ON-driven excitation

(Fig. 3A-D). Reduced GABAergic inhibition by ACh was already observed in hypothalamic VPCs, resulting in increased VP release *in-vitro* [26, 50].

Non ACh-specific silencing of all vesicular release from HDB projections in the OB reduces glomerular activity to odor stimulation *in-vivo* [34]. In addition, optogenetic specific stimulation of HDB cholinergic projections in the OB *in-vivo* increases odor responses in projection neurons [41, 42]. Both results indicate overall excitatory effects of HDB cholinergic modulation in the OB during odor stimulation. Cells in the GL were reported to have a particularly high sensitivity for ACh, and direct application of ACh resulted in both, increase and decrease of spontaneous spiking rates in individual cells there [51]. These bidirectional effects may be explained by the presence of two different ACh receptor subtypes, nicotinic and muscarinic receptors, and their distinct effects on the various cell types of the OB [52]. In our experiments, we demonstrated that both blockade of nicotinic and muscarinic signaling efficiently reduces the percentage of evoked APs in VPCs (Fig. 3I, K). However, only muscarinic blockade can completely block ACh-triggered EPSPs/APs, and IPSP disinhibition (Fig. 3K), indicating that the muscarinic pathway plays the predominant role in VPC excitation. At the level of the GL, it is shown that the muscarinic pathway enhances inhibitory inputs to GABAergic interneurons, i.e. periglomerular cells and short axon cells [31]. According to our data, muscarinic but not nicotinic signaling is responsible for the reduction of ON-evoked IPSP amplitudes in VPCs (Fig. 3I, K). Thus, the disinhibition might be mainly a result of muscarinic receptor-driven inhibition of GABAergic interneurons that are involved in the inhibition of VPCs [8]. However, the origin of the ON-driven excitation that is responsible for triggering APs during ACh application still needs to be identified. Possible candidates would be somatic and lateral dendritic inputs since ON-evoked Ca^{2+} signals in the tuft were not increased in ACh (Fig. 3G).

How is the ACh system activated in the context of social interaction?

If centrifugal cholinergic modulation from the HDB is indeed responsible for increasing VPC activity, the question remains how ACh is released in the OB in a context-dependent manner such as social interaction. Social perception is thought to be a multisensory process as diverse inputs

from the whole stimulus animal are sampled and integrated [4, 10, 11]. In support of this idea, Matsuo et al. [3] showed that genetic ablation of dorsal MOB glomeruli impairs the expected emission of ultrasonic vocalization by male mice towards female urine, whereas these mice still emit ultrasonic vocalizations in the presence of a whole female mouse. This indicates that other sensory stimuli than those provided by olfaction can trigger this social behavior. Moreover, it was shown that rats which were exposed to no more than volatile odors of stimulus rats during the social discrimination paradigm cannot discriminate the different sources of these odors [30]. According to our hypothesis, this impairment might be due to the absence of non-olfactory cues. However, we cannot completely exclude that the absence of supporting pheromonal information also plays a role in this phenomenon. Intriguingly, the HDB or the ACh system in general is activated by various sensations, such as olfactory, visual and tactile stimuli [35, 36, 40]. Stimulation of the HDB cholinergic projections or ACh application in turn can enhance as well as reduce neural activity in all primary sensory cortices [53-55]. Also, especially if the sensation is associated with learning, ACh tends to be released in the respective sensory cortex, for example during conditioning of auditory or tactile cues with food as an unconditioned stimulus [40, 56]. Accordingly, our data demonstrates increased HDB ACh activity in a social memory paradigm (Fig. 4). Thus, it is tempting to speculate that the HDB cholinergic system could play a role as a multisensory integration center during complex contexts like social interaction that provides modulatory feedback to sensory processing, including but not limited to olfaction. Intriguingly, similar multi-sensory integration is also discussed to take place in the insular cortex which is responsible for coordinated behavioral output during social decision-making [57]. From a translational point of view, it is interesting to note that also human research on social behavior deficits suggests a social-context network that integrates social cues (frontal lobe), consolidates social-context associations (temporal lobe), and converges environmental and internal signals (insular lobe) [58].

ACh activity is also correlated with certain internal states in animals, e.g. arousal or attention [37-39]. This internal state-dependent ACh release is triggered by the novelty of stimuli [17, 59]. Rats discriminate individuals according to their social novelty [4]. Thus, we suggest that both multi-sensation and assessing the novelty of rats in the context of social interaction can lead to

increased HDB ACh activity and thereby cholinergic neurotransmission in the OB.

Why is ACh-dependent VP neurotransmission essential for social discrimination?

Our pERK and electrophysiological experiments imply a central role for ACh in VP-dependent social discrimination and accordingly social memory. The involvement of centrifugal ACh as a facilitator of olfactory learning or habituation has been investigated for decades [60]. The blockade of the muscarinic pathway in the OB impairs both aversive and appetitive learning [61, 62]. Intriguingly, it was shown that the blockade of muscarinic neurotransmission in the OB by scopolamine does not impair single-molecule odor recognition [63]. However, non-ACh specific silencing of overall release from HDB projection in the OB impairs social habituation to female conspecific mice [34]. In addition, here we demonstrated that the injection of the muscarinic antagonist, atropine, in the OB efficiently blocks the recognition of a known rat in the social discrimination task (Fig. 5E). Thus, muscarinic neuromodulation in the OB is more important for facilitating the memory of social odor signatures. These findings indicate that social discrimination/habituation and simple odor discrimination/habituation paradigms differ from each other. Regarding sensory complexity, social discrimination recruits multiple senses, whereas odor discrimination is limited to mostly mono-molecular odorants. As mentioned above, multisensory stimulation is a known trigger for the activation of HDB ACh neurons. Atropine-induced impairment of social discrimination was rescued by additional VP injection in the OB (Fig. 5F). Therefore, we suggest that ACh facilitates social discrimination via enabling bulbar VP release. Since bulbar VP signaling is essential for social discrimination but not for simple odor habituation [7], we suggest that bulbar VP is released selectively in a social multisensory context. This hypothesis is supported by a study with another social behavior related neuropeptide, oxytocin, in which Martinon et al. [64] demonstrated that oxytocin release in the bed nucleus of stria terminalis is not increased with a foot shock alone, but when the foot shock is paired with another sensory cue (condition stimulus). Intriguingly, multisensory integration was recently also implied in a context of social discrimination. Accordingly, rats and mice cannot recognize their cage mates if they are immobile due to anesthesia and mice that are both, whiskerless and deaf are not able to

discriminate awake novel and known conspecifics anymore [65]. Moreover, we showed that multisensory social interaction as well as ACh activates bulbar VPCs indicating that ACh activation facilitates context-dependent activation of the bulbar VP system.

The absence of sensitivity to both the muscarinic antagonist or a V1aR knock-down by siRNA in simple odor discrimination and habituation [7, 63] implies that ACh-induced VP signaling is necessary only for discrimination of complex mixtures of odors (e.g. body odors). Indeed, Singer et al. [66] showed that volatile MHC components in mouse urine contain similar compositions of compounds across strains suggesting that volatile MHCs are not distinguishable by the presence or absence of some unique compounds. However, the amplitudes of some prominent compound peaks in the gas chromatogram are different between strains, indicating that mice can recognize the differences of relative concentrations of certain compounds in body odor mixtures. Rats perceive not only volatile urinary odors but also volatile odors from other sources and even differentiate individuals from the same strain during the social discrimination task. Thus, it is likely that the olfactory cues that they can discriminate are even more complex. This idea was also supported by our finding that social interaction results in increased $pERK^+$ MCs in the rat exposure group (Fig. 1D). We therefore suggest that additional bulbar VP neuromodulation is needed to enhance the signal-to-noise ratio of complex odor inputs to allow better identification of individual body odors. Reduced activity of individual projection neurons via increased activity of interneurons is thought to act as a filtering mechanism [67, 68]. Although social interaction increased pERK activation in MCs (Fig. 1D), individual inhibition of $pERK^+$ MCs like reduction of the firing frequency should be still possible. Indeed, it was already shown that VP administration dampens odor-evoked firing of MCs in anesthetized rats [7] and reduces ON-evoked EPSPs in external tufted cells *in-vitro* [8]. Thus, we suggest that this filtering effect facilitated by bulbar VP can interfere weak or quantitatively similar inputs, so that only quantitatively prominent inputs are transmitted to higher brain regions leading to more prominent differences in the neuronal representation of different social odor signatures. This reduction of noise could help the rats to discriminate similar mixtures of body odors during the social discrimination task, but also during social interaction in nature.

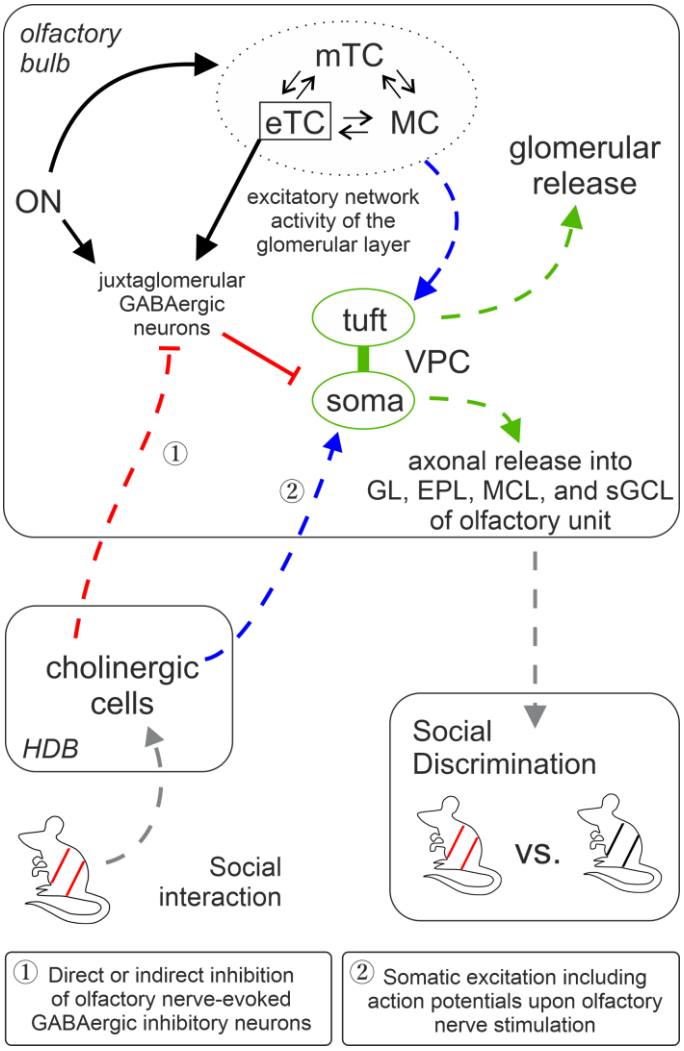

Fig. 6. Graphic summary of olfactory bulb pathways involved in social discrimination

Blue, green, and grey arrows represent excitatory and red lines inhibitory pathways indicated by this study and our previous publication [8]. The cells within the dashed circle indicate the excitatory network within the same home glomerulus. Dashed pathways were confirmed but not fully dissected on the synaptic level. Green pathways are related to vasopressin signaling, grey pathways to sensory input or behavioral output and black pathways are based on findings from literature. EPL, external plexiform layer; eTC, external tufted cell; GL, glomerular layer; HDB, horizontal limb of the diagonal band of broca; MC, mitral cell; MCL, mitral cell layer; mTC, middle tufted cell; ON, olfactory nerve; sGCL, superficial granule cell layer; VPC, vasopressin cell.

Methods

Animals

All experiments were conducted according to national and institutional guidelines for the care and use of laboratory animals, the rules laid down by the EC Council Directive (86/89/ECC), German animal welfare and the local government of Oberpfalz and Unterfranken. Wistar rats of either sex were purchased from Charles River Laboratories (Sulzfeld, Germany) or bred onsite in the animal facilities at the University of Regensburg. Heterozygous VP-eGFP Wister rats [22] of either sex were bred at the University of Regensburg. The light in the rooms was set to an automatic 12 h-cycle (lights on 07:00-19:00).

In-vivo social stimuli exposure experiment

Stimuli exposure

Three cohorts of male VP-eGFP rats (5-6 weeks) were single-housed at least 3 hours before the experiment for habituation to the new environment. Stimuli used were water, juvenile rat urine (collected and mixed from at least 3 juvenile male, stimulus rats) and juvenile rats (3-4 weeks, male non-cage mates). Water and urine (both 50 µl) were applied on filter papers (2 cm x 3 cm). The different stimuli were gently introduced in the cage and the rats were allowed to explore freely. A stimulus exposure lasts 4 min in which the behavior of the rats was video-taped for confirmation of proper stimulus sampling. Rats that did not directly sniff at the filter paper containing water or urine as well as rats that did not perform proper social investigation (sniffing anogenital and head region, for details see Video analysis: Social investigation) were excluded from the experiment. Immediately after the exposure, rats were deeply anesthetized for transcardiac perfusion and fixation of the brain.

Transcardiac perfusion

Rats were deeply anesthetized with an i.p. injection of ketamine-xylazine (100 mg/kg and 10

mg/kg, respectively). The abdomen and the diaphragm were incised to expose the thoracic cavity. After opening the mediastinum, a needle was inserted into the left ventricle. Following incision of the right atrium, 0.1 M PBS pH 7.4 was perfused for 4 min with a speed of 9.5 mL/min by a pump (GZ-07528-30, Cole-Parmer, Wertheim, Germany) followed by 4 % PFA-PBS for 4 min. Rats were decapitated and the whole brains were extracted. Brains were post-fixed in 4 % PFA-PBS overnight at 4 °C and stored in 30 % sucrose-0.1 M PB at 4 °C for at least 2 days then kept at 4 °C until slicing.

Immunohistochemistry

Brains were sliced with a cryostat (CM3050 S, LEICA, Wetzlar, Germany) at approx. -20 °C, then stored in cryoprotectant solution (0.1 M phosphate buffer, 500 mL; Ethylene Glycol, 300 mL; Sucrose, 300 g; Polyvinyl-pyrrolidone, 10 g) at -20 °C until staining. The OB was cut horizontally with a thickness of 30 µm. On average, six slices from one bulb of each experimental rat were used for staining. The HDB (Figure 24-28 (1.08 - 0.60 mm from the Bregma) in the rat brain atlas [69]) was cut coronally with a thickness of 30 µm. Three slices of each experimental rat were used for staining.

All immunohistochemistry procedures were performed in 12 well plates (Corning Incorporated, Corning, NY, USA) with the free-floating method. Slices were washed three times with 0.3 % Triton-X100 in PBS (PBST) for 10 minutes. Then slices were incubated in methanol for 10 minutes at -20 °C. After washing with PBST for 10 minutes, incubation with 0.1 M Glycine in PBS was performed for 20 minutes at room temperature, followed by washing with PBST for 10 minutes. Slices were incubated with the blocking solution for one hour at room temperature. The blocking solution contained 0.2 % of cold water fish skin gelatin (AURION, Wegeningen, Netherlands) and 0.01 % of NaN3 in normal donkey serum (NB-23-00183-1, NeoBiotech, Nanterre, France). Incubation with primary antibodies (see Antibodies) diluted in the blocking solution was carried out for 72 hours at 4 °C. After washing three times with PBST for 10 minutes, secondary antibodies diluted in the blocking solution were added and incubated for two hours at room temperature, followed by washing three times with PBST for 10 minutes. From the

incubation in secondary antibodies on, every procedure was performed in the dark to avoid bleaching fluorescence. For choline acetyltransferase (ChAT) staining, the protocol was modified. Additional blocking by incubation with avidin and biotin (both 0.001% in PB, Sigma-Aldrich, Darmstadt, Germany) for 30 min and a 10 min wash with PBST in between were carried out before incubation with the blocking solution. Moreover, after the last washing with PBST, incubation in streptavidin conjugated with CF488 (1:400 in PBST, #29034, Biotium, Fremont, CA, USA) for two hours at room temperature was carried out. After staining itself, slices were washed three times with PBST for 10 min. Slices were mounted on objective slides (Thermo Fisher Scientific, Waltham, MA, USA) using DAPI fluoro mount-G (Southern Biotech, Birmingham, AL, USA).

Antibodies

Primary antibodies were goat anti-GFP (1:1000, #600-101-215S, Rockland, Limerick, PA, USA), Rabbit anti-P-p44/42 MAPK (1:1000, #9101S, Cell Signaling Technology, Frankfurt am Main, Germany), Sheep Anti-Choline Acetyltransferase (1:125, ab18736, Abcam, Berlin, Germany). Secondary antibodies were Donkey anti-Goat IgG conjugated with CF488 (for GFP, 1:1000, #20016-1, Biotium), Donkey anti-Rabbit IgG conjugated with CF594 (for pERK, 1:1000 for the OB and 1:500 for the HDB, #20152, Biotium), biotinylated Donkey anti-Sheep IgG (for ChAT, 1:250, #20191-1, Biotium). All antibodies were diluted in the blocking solution.

Fluorescent Microscopy

Fluorescent images of the stained slices were obtained using a DM6 B microscope (LEICA) and the software, LAS X (LEICA). DAPI, CF488 and CF633 were stimulated with an exposure time of 300 ms, 300 ms and 500 ms, respectively. Tile-stitching and z-stack of pictures were performed by LAS X. After taking pictures, those were processed by 3D deconvolution or the Lightning & Thunder process (LAS X) to improve the contrast. Pictures were converted to .tif files using Fiji (ImageJ, downloaded from https://imagej.net/Fiji/Downloads) and contrast was adjusted to the

same levels in every picture. Z-stack pictures from approx. 5-6 different z-positions per bulb or rats were used for analysis.

Cell counting

Immunoreactive cells were counted manually using the multi-point tool or cell counter plug-in in Fiji. Double positive cells were identified by comparing two color channels. The position of counted cells was saved as .roi files or .xml files. The number of cells was averaged per experimental rat and bulb.

All the data was analyzed by an observer blinded with respect to stimulation groups.

Electrophysiology

Slice preparation

11-18 day-old juvenile VP-eGFP rats were used for *in vitro* electrophysiology experiments. The rats were deeply anesthetized with isoflurane and quickly decapitated. Horizontal and sagittal slices (300 µm) were cut in ice-cold carbogenized ACSF (artificial cerebrospinal fluid; mM: 125 NaCl, 26 NaHCO3, 1.25 NaH2PO4, 20 glucose, 2.5 KCl, 1 MgCl2, and 2 CaCl2) using a vibratome (VT 1200, LEICA) and afterwards incubated in ACSF at 36 °C for 45 min. Until experiments, the slices were kept at room temperature (approx. 21°C) in ACSF.

Electrophysiology

Brain slices were placed in a recording chamber on the microscope's stage perfused with carbogenized ASCF circulated by a perfusion pump (ISM 850, Cole-Parmer). GFP-labeled vasopressin cells (VPCs) were identified with LED illumination (470 nm) under a modified Zeiss Axioplan microscope (Carl Zeiss Microscopy, Oberkochen, Germany). Epifluorescence was filtered by a long-pass dichroic mirror (490 nm cutoff) and an emission filter (510 ± 21 nm) and visualized with a digital camera (VisiCAM-100, Visitron Systems, Puchheim, Germany). To

perform whole-cell patch-clamp recordings, cells were visualized by infrared gradient-contrast illumination via IR filter (Hoya, Tokyo, Japan). Glass pipettes for recordings were pulled by a pipette puller (Narishige, Tokyo, Japan) sized 4-6 MΩ and filled with intracellular solution (in mM: 130 K-methylsulfate, 10 HEPES, 4 MgCl2, 4 Na2ATP, 0.4 NaGTP, 10 Na Phosphocreatine, 2 ascorbate, pH 7.2). Recordings were performed with the current-clamp configuration using an EPC-10 (HEKA, Lambrecht, Germany) digital oscilloscope. Series resistance was measured 10-30 MΩ. The average resting membrane potential was -50 to -60 mV. Leaky cells with holding current above -50 pA were rejected. Experiments with a drastic drift in the resting membrane potential were rejected as well. Experiments were performed at room temperature (approx. 21°C).

Olfactory nerve stimulation

Olfactory nerve (ON) stimulation was performed with a glass pipette stimulation electrode sized around 2 MΩ. Glass pipettes were filled with ACSF. The electrode was connected to an external stimulator (STG 1004, Multi-Channel Systems, Reutlingen, Germany) controlled by a PC. The stimulation strength was adjusted with the stimulator's software (MC_Stimulus, V 2.1.5) and stimulation was triggered by the amplifier software (Patchmaster, HEKA). Stimulation pipettes were gently placed in the ON layer anterior to a cell to patch using a manual manipulator (LBM-7, Scientifica, East Sussex, UK) under optical control with the microscope. The stimulation strength was 50-400 µA for 100 µs. The stimulation was triggered every 30 s to avoid desensitization of the neural networks.

Ca^{2+} Imaging

Fluorescence was recorded by two-photon laser scanning microscopy on a Femto-2D microscope (Femtonics, Budapest, Hungary), equipped with a tunable, Verdi-pumped Ti:Sa laser (Chameleon Ultra I, Coherent, Glasgow, Scotland). The microscope was equipped with a 60x Nikon Fluor water-immersion objective (NA 1.0; Nikon Instruments, Melville, NY, USA), three detection channels (green fluorescence (epi and trans), red (epi) and infrared light (trans)) and

controlled by MES v4.5.613 software (Femtonics).

VP-eGFP cells were identified in the green channel at an excitation wavelength of 950 nm. VPC bodies were patched in the whole-cell mode with patch pipettes filled with regular intracellular solution (see Electrophysiology), Alexa Fluor 549 (50 µM, Invitrogen) and the Ca^{2+} indicator OGB-1 (100 µM, Invitrogen, Thermo Fisher Scientific) were added for neurite visualization and Ca^{2+} imaging. Fluorescence transients and image stacks were acquired at 800 nm laser excitation. Data were mostly collected from the medial surface of the OB. Ca^{2+} imaging experiments were performed at room temperature (approx. 21° C). The patched VPCs were held in the current clamp mode near their resting potential of -55 mV. Again, leaky VPCs with a holding current beyond -50 pA were dismissed. A shift in baseline fluorescence F_0 of more than 15 % between the first and the last measurement of each region of interest (ROI) also led to a rejection of the experiment. Structures of interest were imaged in free line-scanning mode with a temporal resolution of approx. 1 ms.

Experimental design and data analysis

All drugs (see Pharmacology) diluted in ASCF were bath-applied via the perfusion system. Recordings under pharmacology were performed at least 5 min after the onset of administration to ensure that the drugs reached the recorded cell. Two average traces from 3-5 recordings in each condition were analyzed. The data was averaged per condition. The amplitudes of PSPs were measured using Origin 2018b (Origin Lab). The amplitudes of IPSPs following pharmacology were normalized to the amplitudes during the ACSF condition (100 %). The amplitudes of EPSPs following bicuculline application with pharmacology were normalized to the amplitudes during the bicuculline condition (100%). APs, EPSPs, IPSPs in experiments with ACh application were defined as: APs, the existence of AP (s) after ON stimulation; EPSPs, observation of depolarization with amplitudes of >1.5 mV; IPSPs, observation of hyperpolarization with amplitudes of >1.5 mV. In some experiments with ACh, current (40, 60, 80, 100 pA, 600 ms) was injected via the recording electrode into the cell to test if ACh application alters the intrinsic excitability in VPCs. Spiking rates of AP trains were calculated as the number of spikes divided by

the duration of AP trains. Latency of the first spike was measured as the duration between the current injection onset and the peak of the first spike.

In some experiments, simultaneous to the electrophysiological recordings, intracellular Ca^{2+} transients were measured at the tuft and at the apical dendrite directly apical to the soma (see Ca^{2+} Imaging) following ON stimulation. Three consecutive focal line-scans were performed during ON stimulation (see Olfactory nerve stimulation). To confirm that the cell was correctly filled with Ca^{2+}-dye, VPCs were also stimulated with somatic 50 Hz trains (20 APs) via the patch pipette which was shown to reliably trigger Ca^{2+} Influx in case ON stimulation did not result in Ca^{2+} signals near the soma during olfactory nerve stimulation [8]. The three line scans per pharmacological condition were averaged for analysis. Dendritic Ca^{2+} transients were analyzed in terms of $\Delta F/F$ relative to the resting fluorescence F_0 [70]. The time course of pharmacology and analysis were the same as for electrophysiological data mentioned above.

All the data was analyzed by an observer blinded with respect to pharmacology.

Pharmacology

All pharmacological agents used were diluted in ACSF for bath application: serotonin hydrochloride (20 µM, Sigma-Aldrich), DL-Norepinephrine hydrochloride (20 µM, Sigma-Aldrich), acetylcholine chloride (100 µM, Sigma-Aldrich), mecamylamine hydrochloride (20 µM, Sigma-Aldrich), atropine (10 µM, Sigma-Aldrich), 1(S),9(R)-(-)-bicuculline methyl bromide (50 µM, Sigma-Aldrich).

The doses used were chosen based on minimal doses reported to elicit *in-vitro* effects [8, 26-28, 31, 71].

Behavioral Pharmacology

Cannula implantation

Three cohorts of 5-6 week-old male Wistar rats were group-housed until surgery. To allow local injection of pharmacological solutions in the OB without anesthesia, we bilaterally implanted

guide cannulae (23 G) 2 mm above the injection coordinates in the rat OB. The coordinates for injection were 7 mm anterior and 1.2 mm lateral relative to bregma as well as and 3 mm ventral to the surface of the skull[69]. Before surgery, all surgical instruments were autoclaved at 121 °C for 20 min. The rats were anesthetized by isoflurane using a TEC 3 isoflurane vaporizer (Eickemeyer, Tuttlingen, Germany). The concentration of isoflurane was maintained between 2-3 %. The rats were fixed on a stereotaxic frame (TSE, Bad Homburg Germany/Kopf, Tujunga, CA, USA) using ear bars. To prevent hypothermia, the rats were kept warm using a warming pad (ThermoLux, Witte + Sutor, Murrhardt, Germany). Analgetics (buprenorphine, 0.1 mg/kg s.c., Bayer, Beline, Germany) and antibiotics (enrofloxacin, 10 mg/kg s.c., Bayer) were injected before surgery. After shaving the head and disinfection of the operation site with 70 % ethanol, we incised the scalp and the supporting tissue on the skull. Injection of lidocaine hydrochloride (2 %, around 100 µL, bela-pharm, Vechta, Germany) under the scalp was operated if needed. Two stainless steel jeweler's screws were inserted into the skull using a surgical drill (NM 3000, NOUVAG, Goldach, Switzerland). One on the left anterior to bregma and the other one on the right posterior to bregma to secure dental cement fixation. Holes for guide cannulae were made by a drill, followed by placement of cannulae 1 mm ventral from the surface of the skull. Cannulae and the two screws were fixed together by the dental cement. Once the cement dried, the connection between the cement and the scalp was disinfected by iodine solution and cannulae were blocked by insertion of stainless steel stylets (25 G) to prevent dust entering the cannulae that could result in infection or blockage. The rats were removed from the frame and placed in fresh cages for recovering from anesthesia under observation until they are awake. The rats were weighed prior to surgery and on the next day to see if they recovered properly after surgery. Their health condition and behavior were checked for at least five days. After surgery, they were single-housed until experiments to prevent damage to the guide cannulae. Meanwhile, the rats were handled and habituated to the removal and insertion of stylets every day until experiments. Stylets were cleaned with 70 % ethanol every time they were removed from the guide cannula.

Social discrimination with pharmacology

We combined the social discrimination paradigm [4] and microinjection of pharmacology into the OB. The social discrimination paradigm consists of a sampling phase and a discrimination phase. Experiments were performed in the afternoon. In the sampling phase (4 min), one stimulus rat was gently introduced into the cage of the experimental rats. Then the stimulus rat was removed from the cage and the experimental rat stayed in the cage alone for an inter-exposure interval of 30 min. In the discrimination phase (4 min), two stimulus rats, one is the same as during the sampling phase and the other one is a novel stimulus rat, were gently introduced into the cage. During both phases, the behavior of the experimental rat was video-taped from above through a transparent plastic plate for post-hoc analysis. Stimuli were 3-4 week-old group-housed male rats that were single-housed only in between the social exposures of the behavioral experiments to prevent mixing of body odors. They were marked with a red or black pen of the same brand (Edding, Ahrensburg, Germany) to allow visual differentiation by the observers. Pharmacological agents diluted in ACSF include atropine (1 µg in 1 µL) and [Arg8]-vasopressin acetate salt (1 ng in 1 µL, Sigma-Aldrich). 40 min before the sampling phase, either ACSF or atropine was injected into both OB hemispheres (1 µL each). 10 min before the sampling phase, either ACSF or VP was injected into both OB hemispheres (1 µL each). All injections were carried out with microinjection syringes (Hamilton, Bonaduz, Switzerland) connected to a self-made injection system which consists of plastic tubes and 10 mm-long 30 G needles (2 mm longer than the guide cannulae). After every injection (1 µL), the injection systems rested in place for 1 min to allow the injected solution to diffuse fully in the tissue. The doses used were chosen based on minimal does reported to elicit behavioral effects [6, 72]. No anatomical outliers in stereotaxic cannula implantation had to be excluded from behavioral analysis (Fig. 5). However, one animal from the control group was removed, as it showed a high amount of unspecific sexual/mounting behavior towards the stimulus animals throughout the sampling as well as the discrimination phase.

Confirmation of injection sites

Immediately after the last experiments, the rats were killed with CO_2. Then 1 µl of blue ink was

injected with an injection system via the guide cannulae into both OBs followed by decapitation. The OB was extracted and quickly frozen in isobutanol on dry ice and stored at -20 °C until use. Correct placement of Injection was identified on 40 µm cryostat sagittal sections stained with cresyl violet (Fig. 5C). No anatomical outliers in stereotaxic cannula implantation had to be excluded from behavioral analysis.

Video analysis: Social investigation

The analysis was done by an observer blind to the pharmacological treatment using JWatcher (downloaded from https://www.jwatcher.ucla.edu/). Thereby the duration of investigation of the stimulus rats by the experimental rats was measured. Investigation was defined as sniffing the anogenital or neck region of stimulus rats including obvious nose movements ("sniffing"). Aggressive behavior (e.g. aggressive grooming), only staying next to the stimulus rats, and rough and tumble play were where not considered investigation [4] (Fig. 5B). One animal from the control group was removed, as it showed high amounts of unspecific sexual/mounting behavior towards the stimulus animals throughout the sampling as well as the discrimination phase.

Statistical analysis

Statistics were performed with SPSS (ver. 26, IBM, Armonk, NY, USA) and G*Power (ver. 3.1.9.2, Franz Faul, University of Kiel). All statistical analysis performed was two-sided and significance was accepted at $p<0.05$. Type of statistic was determined using the Kolmogorov-Smirnov test for normal distribution in SPSS. Effect sizes for parametric statistics (Cohen's *d, dz*, *f*) were determined using SPSS and G*Power. Effect sizes for non-parametric statistics were calculated from z-scores (Pearson's r = $|z|/\sqrt{n}$) [73]. Sample sizes were either based on prior studies or an a priori power analysis. Power and sample sizes (for α=0.05) were determined using G*Power.
All Ns indicate biological replication, that is, data from different samples (different cells or different animals). To better illustrate replication in acute in-vitro slice experiments it is also clearly indicated in the results section from how many different animals the measurements originate from.

For complete details concerning type of statistic (parametric or non-parametric), type of test, test statistics (F, t, W, U, z-score), degrees of freedom, p-value, effect size, and achieved power of every statistical analysis performed in the result section see table 1. Figure identifiers and lower case arabic letters in the table represent affiliation to the statistical data represented in the figures and the text, respectively.

All Ns indicate biological replication, that is, data from different samples (different cells or different animals). To illustrate replication in acute in-vitro slice experiments it is also clearly indicated in the results section from how many different animals the measurements originate from.

Data availability statement:

All numerical data that is represented in the figures is available as source data file corresponding to the figures.

Acknowledgments

The work was supported by the German research foundation (DFG LU2164/1-1 and EG 135/5-1). We thank Anne Pietryga-Krieger and Dr. Max Müller for experimental support and Dr. Mike Ludwig (University of Edinburgh) for providing the VP-eGFP rats. We also thank Prof. Inga Neumann for providing video equipment and stereotactic instruments for the behavioral pharmacology experiments and Dr. Vinicius Oliveira for critically reading the manuscript

Author contributions

H.S. and M.L. designed research; M.L. and H.S. performed research; M.L. and H.S. analyzed data; V.E. provided advice on the design and analysis of electrophysiology and Ca^{2+} imaging experiments; H.S. wrote the first draft of the manuscript. H.S., V.E. and M.L. wrote and revised the manuscript.

Competing interests

The authors declare no competing financial interest

Table 1 **Statistical overview**

	Figure	Type of statistic	Type of test	Test statistic	P-value	Effect size	Power
a	1B	parametric	One-way ANOVA	$F_{(2,26)}$=0.406	p=0.670	*f*=0.176	0.115
b	1C	parametric	One-way ANOVA and post-hoc (LSD) rat vs water rat vs urine urine vs. water	$F_{(2,26)}$=6.156 - -	p=0.006 p=0.020 p=0.047	*f*=0.688 *d*=1.300 *d*=0.617	0.888
c	1D	parametric	One-way ANOVA and post-hoc (LSD) rat vs water rat vs urine urine vs. water	$F_{(2,26)}$=3.586 - - -	p=0.042 p=0.025 p=0.034 p=0.949	*f*=0.525 *d*=1.117 *d*=0.824 *d*=0.232	0.663
d	S1B	parametric	One-way ANOVA	$F_{(2,24)}$=0.633	p=0.539	*f*=0.229	0.156
e	S1C	parametric	One-way ANOVA and post-hoc (LSD) rat vs water rat vs urine urine vs. water	$F_{(2,24)}$=3.832 - - -	p=0.036 p=0.019 p=0.033 p=0.804	*f*=0.565 *d*=1.152 *d*=0.993 *d*=0.133	0.693
f	S1D	parametric	One-way ANOVA	$F_{(2,24)}$=1.952	p=0.164	*f*=0.403	0.404
g	2C	non-parametric	Related samples Wilcoxon test	$W_{(8)}$=0; z=-2.521	p=0.012	*r*=0.891	0.995
h	2E	non-parametric	Related samples Wilcoxon test	$W_{(9)}$=1; z=-2.547	p=0.011	*r*=0.849	0.984
i	2G	non-parametric	Related samples Wilcoxon test	$W_{(20)}$=0; z=-3.920	p<0.001	*r*=0.876	1.000
j	2H	non-parametric	Mann-Whitney-U test	z=-4.652	p<0.001	*r*=0.736	1.000
k	2I	non-parametric	Kruskal Wallis and post-hoc (Bonferroni) 5-HT vs NA ACh vs 5-HAT ACh vs NA	H=17.439, df=2 z=0.003 z=-3.433 z=-3.291	p<0.001 p=1.000 p=0.003 p=0.002	- *r*=0.001 *r*=0.649 *r*=0.611	- 0.050 0.991 0.980
l	S2A	parametric	(2) × (2) mixed model ANOVA (intensity [within subject] × treatment [within-subject])	$F_{(3, 27)}$=22.14 $F_{(1, 9)}$=0.725 $F_{(3,27)}$=0.588 (interaction)	p<0.001 p=0.417 p=0.528	*f*=0.285 *f*=1.569 *f*=0.255	1.000 1.000 1.000
m	S2B	parametric	(2) × (2) mixed model ANOVA (intensity [within subject] × treatment [within-subject]) ACh vs. ACSF with 40 pA	$F_{(3, 27)}$=49.81 $F_{(1, 9)}$=3.887 $F_{(3,27)}$=6.664 (interaction) -	p<0.001 p=0.080 p=0.015 p=0.029	*f*=0.847 *f*=0.302 *f*=0.860 *d*=2.588	1.000 1.000 1.000
n	3B	non-parametric	Related samples Wilcoxon test	$W_{(5)}$=0; z=-2.023	p=0.043	*r*=0.905	0.872
o	3D	non-parametric	Related samples Wilcoxon test	$W_{(5)}$=0; z=2.023	p=0.043	*r*=0.905	0.872
p	-	non-parametric	Mann-Whitney-U test	$U_{(19)}$=4.0; z=3.121	p=0.002	*r*=0.716	0.988
q	3G	parametric	(2) × (2) mixed model ANOVA (location [within subject] × treatment [within-subject])	$F_{(1,7)}$=17.8 $F_{(1,7)}$=1.98 $F_{(1,7)}$=0.014 (interaction)	p=0.004 p=0.203 p=0.910	*f*=1.596 *f*=0.531 *f*=0.045	1.000 1.000 0.081
r	3I	non-parametric	Friedman test and post-hoc (Dunn) Mecamylamine/ACh vs Mecamylamine Mecamylamine/ACh vs ACSF Mecamylamine vs ACSF	$\chi2$=6.750, df=2 z=2.250 z=-2.250 z=0.000	p=0.034 p=0.024 p=0.024 p=1.000	- *r*=0.795 *r*=0.795 *r*=0.000	- 0.868 0.868 0.050
s	3K	non-parametric	Friedman test	$\chi2$=3.714, df=2	p=0.156	-	-
t	4B	parametric	One-way ANOVA	$F_{(2,13)}$=2.701	p=0.104	*f*=0.645	0.526
u	4C	parametric	One-way ANOVA and post-hoc (LSD) rat vs water rat vs urine urine vs. water	$F_{(2,13)}$=4.411 - - -	p=0.034 p=0.113 p=0.011 p=0.255	*f*=0.823 *d*=0.918 *d*=1.826 *d*=0.933	0.748
v	5D	parametric	Paired samples t-test	$t_{(12)}$=-2.411	p=0.033	*dz*=0.709	0.651
w	5E	parametric	Paired samples t-test	$t_{(13)}$=-1.231	p=0.240	*dz*=0.202	0.208
x	5F	parametric	Paired samples t-test	$t_{(13)}$=-2.420	p=0.031	*dz*=0.647	0.647

Type of statistic was determined using the Kolmogorov- Smirnov test in SPSS. Tests were performed using SPSS. Effect sizes for parametric statistics were determined using SPSS and G*Power (Cohen's *d, dz*, *f*). Effect sizes for non-parametric statistics were calculated from z-scores (Pearson's r = $|z|/\sqrt{n}$) [73]. Power (for α=0.05) was determined using G*Power.

References

1. Baldwin B, Shillito EE. The effects of ablation of the olfactory bulbs on parturition and maternal behaviour in Soay sheep. Animal Behaviour. 1974;22(1):220-3. doi: 10.1016/S0003-3472(74)80072-2.

2. Williams JR, Slotnick BM, Kirkpatrick BW, Carter CS. Olfactory-Bulb Removal Affects Partner Preference Development and Estrus Induction in Female Prairie Voles. Physiology & Behavior. 1992;52(4):635-9. doi: 10.1016/0031-9384(92)90390-N. PubMed PMID: WOS:A1992JT02000003.

3. Matsuo T, Hattori T, Asaba A, Inoue N, Kanomata N, Kikusui T, et al. Genetic dissection of pheromone processing reveals main olfactory system-mediated social behaviors in mice. P Natl Acad Sci USA. 2015;112(3):E311-E20. doi: 10.1073/pnas.1416723112. PubMed PMID: WOS:000348040700012; PubMed Central PMCID: PMC4311817.

4. Engelmann M, Hadicke J, Noack J. Testing declarative memory in laboratory rats and mice using the nonconditioned social discrimination procedure. Nature Protocols. 2011;6(8):1152-62. doi: 10.1038/nprot.2011.353. PubMed PMID: WOS:000294480300006.

5. Lukas M, Neumann ID. Oxytocin and vasopressin in rodent behaviors related to social dysfunctions in autism spectrum disorders. Behav Brain Res. 2013;251:85-94.

6. Dluzen DE, Muraoka S, Engelmann M, Landgraf R. The effects of infusion of arginine vasopressin, oxytocin, or their antagonists into the olfactory bulb upon social recognition responses in male rats. Peptides. 1998;19(6):999-1005. doi: 10.1016/S0196-9781(98)00047-3. PubMed PMID: WOS:000075014900005.

7. Tobin VA, Hashimoto H, Wacker DW, Takayanagi Y, Langnaese K, Caquineau C, et al. An intrinsic vasopressin system in the olfactory bulb is involved in social recognition. Nature. 2010;464(7287):413-U110. doi: 10.1038/nature08826. PubMed PMID: WOS:000275657100047; PubMed Central PMCID: PMC2842245.

8. Lukas M, Suyama H, Egger V. Vasopressin Cells in the Rodent Olfactory Bulb Resemble Non-Bursting Superficial Tufted Cells and Are Primarily Inhibited upon Olfactory Nerve Stimulation. eneuro. 2019;6(4):ENEURO.0431-18.2019. doi: 10.1523/eneuro.0431-18.2019.

9. Halász N. The Vertebrate Olfactory System: Chemical neuroanatomy, function and development. Budapest: Akadémiai Kiadó; 1990.

10. Bobrov E, Wolfe J, Rao RP, Brecht M. The Representation of Social Facial Touch in Rat Barrel Cortex. Current Biology. 2014;24(1):109-15. doi: 10.1016/j.cub.2013.11.049. PubMed PMID: WOS:000329501400033.

11. Rao RP, Mielke F, Bobrov E, Brecht M. Vocalization–whisking coordination and multisensory integration of social signals in rat auditory cortex. Elife. 2014;3:e03185. doi: 10.7554/eLife.03185.

12. Shipley MT, Halloran FJ, Delatorre J. Surprisingly Rich Projection from Locus Coeruleus to the Olfactory-Bulb in the Rat. Brain Research. 1985;329(1-2):294-9. doi: Doi 10.1016/0006-8993(85)90537-2. PubMed PMID: WOS:A1985AED8400032.

13. McLean JH, Shipley MT. Serotonergic afferents to the rat olfactory bulb: I. Origins and laminar specificity of serotonergic inputs in the adult rat. J Neurosci. 1987;7(10):3016-28.

14. Ojima H, Yamasaki T, Kojima H, Akashi A. Cholinergic Innervation of the Main and the Accessory Olfactory Bulbs of the Rat as Revealed by a Monoclonal-Antibody against Choline-Acetyltransferase. Anatomy and Embryology. 1988;178(6):481-8. doi: Doi 10.1007/Bf00305035. PubMed PMID: WOS:A1988Q065600002.

15. Popova NK, Amstislavskaya TG. 5-HT2A and 5-HT2C serotonin receptors differentially modulate mouse sexual arousal and the hypothalamo-pituitary-testicular response to the presence of

a female. Neuroendocrinology. 2002;76(1):28-34. doi: 10.1159/000063681. PubMed PMID: WOS:000176986900004.

16. Purvis EM, Klein AK, Ettenberg A. Lateral habenular norepinephrine contributes to states of arousal and anxiety in male rats. Behavioural Brain Research. 2018;347:108-15. doi: 10.1016/j.bbr.2018.03.012. PubMed PMID: WOS:000436916800013.

17. Acquas E, Wilson C, Fibiger HC. Conditioned and unconditioned stimuli increase frontal cortical and hippocampal acetylcholine release: Effects of novelty, habituation, and fear. Journal of Neuroscience. 1996;16(9):3089-96. doi: 10.1523/JNEUROSCI.16-09-03089.1996. PubMed PMID: WOS:A1996UF71100022.

18. Prado VF, Martins-Silva C, de Castro BM, Lima RF, Barros DM, Amaral E, et al. Mice deficient for the vesicular acetylcholine transporter are myasthenic and have deficits in object and social recognition. Neuron. 2006;51(5):601-12. doi: 10.1016/j.neuron.2006.08.005. PubMed PMID: WOS:000240623400009.

19. Dluzen DE, Muraoka S, Landgraf R. Olfactory bulb norepinephrine depletion abolishes vasopressin and oxytocin preservation of social recognition responses in rats. Neuroscience Letters. 1998;254(3):161-4. doi: 10.1016/S0304-3940(98)00691-0. PubMed PMID: WOS:000076397000010.

20. Cavalcante LES, Zinn CG, Schmidt SD, Saenger BF, Ferreira FF, Furini CRG, et al. Modulation of the storage of social recognition memory by neurotransmitter systems in the insular cortex. Behavioural Brain Research. 2017;334:129-34. doi: 10.1016/j.bbr.2017.07.044. PubMed PMID: WOS:000411302200016.

21. Sawyer TF, Hengehold AK, Perez WA. Chemosensory and Hormonal Mediation of Social Memory in Male-Rats. Behavioral Neuroscience. 1984;98(5):908-13. doi: 10.1037/0735-7044.98.5.908. PubMed PMID: WOS:A1984TM41200016.

22. Ueta Y, Fujihara H, Serino R, Dayanithi G, Ozawa H, Matsuda K, et al. Transgenic expression of enhanced green fluorescent protein enables direct visualization for physiological studies of vasopressin neurons and isolated nerve terminals of the rat. Endocrinology. 2005;146(1):406-13. doi: 10.1210/en.2004-0830. PubMed PMID: WOS:000225766500054.

23. Bluthe RM, Dantzer R. Role of the Vomeronasal System in Vasopressinergic Modulation of Social Recognition in Rats. Brain Research. 1993;604(1-2):205-10. doi: 10.1016/0006-8993(93)90370-3. PubMed PMID: WOS:A1993KN96000026.

24. Le Jeune H, Aubert I, Jourdan F, Quirion R. Comparative laminar distribution of various autoradiographic cholinergic markers in adult rat main olfactory bulb. Journal of chemical neuroanatomy. 1995;9(2):99-112. doi: 10.1016/0891-0618(95)00070-N.

25. Yuan Q, Harley CW, McLean JH. Mitral cell β1 and 5-HT2A receptor colocalization and cAMP coregulation: A new model of norepinephrine-induced learning in the olfactory bulb. Learning & memory. 2003;10(1):5-15. doi: 10.1101/lm.54803.

26. Li DP, Pan YZ, Pan HL. Acetylcholine attenuates synaptic GABA release to supraoptic neurons through presynaptic nicotinic receptors. Brain Research. 2001;920(1-2):151-8. doi: 10.1016/S0006-8993(01)03055-4. PubMed PMID: WOS:000172791300017.

27. Liu S, Aungst JL, Puche AC, Shipley MT. Serotonin modulates the population activity profile of olfactory bulb external tufted cells. Journal of neurophysiology. 2011;107(1):473-83. doi: 10.1152/jn.00741.2011.

28. Zimnik NC, Treadway T, Smith RS, Araneda RC. α1A‐Adrenergic regulation of inhibition in the olfactory bulb. The Journal of physiology. 2013;591(7):1631-43. doi: 10.1113/jphysiol.2012.248591.

29. Vargas-Barroso V, Ordaz-Sánchez B, Peña-Ortega F, Larriva-Sahd JA. Electrophysiological Evidence for a Direct Link between the Main and Accessory Olfactory Bulbs in the Adult Rat. Frontiers

in Neuroscience. 2016;9:518. doi: 10.3389/fnins.2015.00518. PubMed PMID: 26858596; PubMed Central PMCID: PMC4726767.

30. Noack J, Richter K, Laube G, Haghgoo HA, Veh RW, Engelmann M. Different importance of the volatile and non-volatile fractions of an olfactory signature for individual social recognition in rats versus mice and short-term versus long-term memory. Neurobiology of Learning and Memory. 2010;94(4):568-75. doi: 10.1016/j.nlm.2010.09.013. PubMed PMID: WOS:000284298700016.

31. Liu SL, Shao ZY, Puche A, Wachowiak M, Rothermel M, Shipley MT. Muscarinic Receptors Modulate Dendrodendritic Inhibitory Synapses to Sculpt Glomerular Output. Journal of Neuroscience. 2015;35(14):5680-92. doi: 10.1523/Jneurosci.4953-14.2015. PubMed PMID: WOS:000353054900020.

32. Shipley MT, Ennis M. Functional organization of olfactory system. Journal of Neurobiology. 1996;30(1):123-76. doi: 10.1002/(sici)1097-4695(199605)30:1<123::aid-neu11>3.0.co;2-n. PubMed PMID: WOS:A1996UF05000011.

33. Senut M, Menetrey D, Lamour Y. Cholinergic and peptidergic projections from the medial septum and the nucleus of the diagonal band of Broca to dorsal hippocampus, cingulate cortex and olfactory bulb: a combined wheatgerm agglutinin-apohorseradish peroxidase-gold immunohistochemical study. Neuroscience. 1989;30(2):385-403. doi: 10.1016/0306-4522(89)90260-1.

34. Schwarz I, Müller M, Pavlova I, Schweihoff J, Musacchio F, Mittag M, et al. The diagonal band of broca continually regulates olfactory-mediated behaviors by modulating odor-evoked responses within the olfactory bulb. bioRxiv. 2020:2020.11.07.372649. doi: 10.1101/2020.11.07.372649.

35. Linster C, Hasselmo ME. Neural activity in the horizontal limb of the diagonal band of Broca can be modulated by electrical stimulation of the olfactory bulb and cortex in rats. Neuroscience Letters. 2000;282(3):157-60. doi: 10.1016/S0304-3940(00)00885-5. PubMed PMID: WOS:000086292300009.

36. Zhu XO, Brown MW, Mccabe BJ, Aggleton JP. Effects of the Novelty or Familiarity of Visual-Stimuli on the Expression of the Immediate-Early Gene C-Fos in Rat-Brain. Neuroscience. 1995;69(3):821-9. doi: 10.1016/0306-4522(95)00320-I. PubMed PMID: WOS:A1995TE43100013.

37. McKenna JT, Cordeira JW, Jeffrey BA, Ward CP, Winston S, McCarley RW, et al. c-Fos protein expression is increased in cholinergic neurons of the rodent basal forebrain during spontaneous and induced wakefulness. Brain Research Bulletin. 2009;80(6):382-8. doi: 10.1016/j.brainresbull.2009.08.015. PubMed PMID: WOS:000271847600010; PubMed Central PMCID: PMCPMC2782706.

38. Imperato A, Puglisiallegra S, Scrocco MG, Casolini P, Bacchi S, Angelucci L. Cortical and Limbic Dopamine and Acetylcholine-Release as Neurochemical Correlates of Emotional Arousal in Both Aversive and Non-Aversive Environmental-Changes. Neurochemistry International. 1992;20:S265-S70. PubMed PMID: WOS:A1992HL80300051.

39. Passetti F, Dalley JW, O'connell MT, Everitt BJ, Robbins TW. Increased acetylcholine release in the rat medial prefrontal cortex during performance of a visual attentional task. European Journal of Neuroscience. 2000;12(8):3051-8. doi: 10.1046/j.1460-9568.2000.00183.x. PubMed PMID: WOS:000089055100038.

40. Butt AE, Testylier G, Dykes RW. Acetylcholine release in rat frontal and somatosensory cortex is enhanced during tactile discrimination learning. Psychobiology. 1997;25(1):18-33. doi: 10.3758/BF03327024. PubMed PMID: WOS:A1997WQ80000003.

41. Bohm E, Brunert D, Rothermel M. Input dependent modulation of olfactory bulb activity by HDB GABAergic projections. Scientific Reports. 2020;10(1):1-15. doi: 10.1038/s41598-020-67276-z. PubMed PMID: WOS:000546550700010.

42. Rothermel M, Carey RM, Puche A, Shipley MT, Wachowiak M. Cholinergic Inputs from Basal Forebrain Add an Excitatory Bias to Odor Coding in the Olfactory Bulb. Journal of Neuroscience. 2014;34(13):4654-64. doi: 10.1523/Jneurosci.5026-13.2014. PubMed PMID: WOS:000333674200022.

43. Anagnostaras SG, Murphy GG, Hamilton SE, Mitchell SL, Rahnama NP, Nathanson NM, et al. Selective cognitive dysfunction in acetylcholine M-1 muscarinic receptor mutant mice. Nature Neuroscience. 2003;6(1):51-8. doi: 10.1038/nn992. PubMed PMID: WOS:000180089300015.

44. Watanabe S, Hoffman DA, Migliore M, Johnston D. Dendritic K+ channels contribute to spike-timing dependent long-term potentiation in hippocampal pyramidal neurons. P Natl Acad Sci USA. 2002;99(12):8366-71. doi: 10.1073/pnas.122210599. PubMed PMID: WOS:000176217700101.

45. Kohno T, Wang HB, Amaya F, Brenner GJ, Cheng JK, Ji RR, et al. Bradykinin enhances AMPA and NMDA receptor activity in spinal cord dorsal horn neurons by activating multiple kinases to produce pain hypersensitivity. Journal of Neuroscience. 2008;28(17):4533-40. doi: 10.1523/Jneurosci.5349-07.2008. PubMed PMID: WOS:000255301100028.

46. Wacker DW, Engelmann M, Tobin VA, Meddle SL, Ludwig M. Vasopressin and social odor processing in the olfactory bulb and anterior olfactory nucleus. Ann Ny Acad Sci. 2011;1220:106-16. doi: 10.1111/j.1749-6632.2010.05885.x. PubMed PMID: WOS:000293198000011.

47. Haga S, Hattori T, Sato T, Sato K, Matsuda S, Kobayakawa R, et al. The male mouse pheromone ESP1 enhances female sexual receptive behaviour through a specific vomeronasal receptor. Nature. 2010;466(7302):118-U36. doi: 10.1038/nature09142. PubMed PMID: WOS:000279343800046.

48. Hattori T, Osakada T, Matsumoto A, Matsuo N, Haga-Yamanaka S, Nishida T, et al. Self-Exposure to the Male Pheromone ESP1 Enhances Male Aggressiveness in Mice. Current Biology. 2016;26(9):1229-34. doi: 10.1016/j.cub.2016.03.029. PubMed PMID: WOS:000375413700031.

49. Kaba H, Rosser A, Keverne B. Neural Basis of Olfactory Memory in the Context of Pregnancy Block. Neuroscience. 1989;32(3):657-62. doi: 10.1016/0306-4522(89)90287-X. PubMed PMID: WOS:A1989CC44800010.

50. Gregg CM. The Compartmentalized Hypothalamo-Neurohypophysial System: Evidence for a NeurohypophysialAction of Acetylcholine on Vasopressin Release. Neuroendocrinology. 1985;40(5):423-9. doi: 10.1159/000124108.

51. Ravel N, Akaoka H, Gervais R, Chouvet G. The Effect of Acetylcholine on Rat Olfactory-Bulb Unit-Activity. Brain Research Bulletin. 1990;24(2):151-5. doi: 10.1016/0361-9230(90)90199-A. PubMed PMID: WOS:A1990CU02200001.

52. Matsutani S, Yamamoto N. Centrifugal innervation of the mammalian olfactory bulb. Anatomical Science International. 2008;83(4):218-27. doi: 10.1111/j.1447-073X.2007.00223.x. PubMed PMID: WOS:000260749600005.

53. Chaves-Coira I, Rodrigo-Angulo ML, Nunez A. Bilateral Pathways from the Basal Forebrain to Sensory Cortices May Contribute to Synchronous Sensory Processing. Frontiers in Neuroanatomy. 2018;12:5. doi: 10.3389/fnana.2018.00005. PubMed PMID: WOS:000423068000002.

54. Kirkwood A, Rozas C, Kirkwood J, Perez F, Bear MF. Modulation of long-term synaptic depression in visual cortex by acetylcholine and norepinephrine. Journal of Neuroscience. 1999;19(5):1599-609. doi: 10.1523/JNEUROSCI.19-05-01599.1999. PubMed PMID: WOS:000078672300006.

55. Metherate R, Ashe JH. Synaptic-Interactions Involving Acetylcholine, Glutamate, and Gaba in Rat Auditory-Cortex. Experimental Brain Research. 1995;107(1):59-72. PubMed PMID: WOS:A1995TH21900008.

56. Butt AE, Chavez CM, Flesher MM, Kinney-Hurd BL, Araujo GC, Miasnikov AA, et al. Association learning-dependent increases in acetylcholine release in the rat auditory cortex during auditory classical conditioning. Neurobiology of Learning and Memory. 2009;92(3):400-9. doi: 10.1016/j.nlm.2009.05.006. PubMed PMID: WOS:000277532500015.

57. Rogers-Carter MM, Christianson JP. An insular view of the social decision-making network.

Neurosci Biobehav R. 2019;103:119-32. doi: 10.1016/j.neubiorev.2019.06.005. PubMed PMID: WOS:000483424200013.

58. Baez S, García AM, Ibanez A. The Social Context Network Model in Psychiatric and Neurological Diseases. In: Wöhr M, Krach S, editors. Social Behavior from Rodents to Humans: Neural Foundations and Clinical Implications. Cham: Springer International Publishing; 2017. p. 379-96.

59. Giovannini MG, Rakovska A, Benton RS, Pazzagli M, Bianchi L, Pepeu G. Effects of novelty and habituation on acetylcholine, GABA, and glutamate release from the frontal cortex and hippocampus of freely moving rats. Neuroscience. 2001;106(1):43-53. doi: 10.1016/S0306-4522(01)00266-4. PubMed PMID: WOS:000171242700005.

60. Wilson DA, Fletcher ML, Sullivan RM. Acetylcholine and olfactory perceptual learning. Learning & Memory. 2004;11(1):28-34. doi: 10.1101/lm.66404. PubMed PMID: WOS:000188646800004.

61. Ravel N, Elaagouby A, Gervais R. Scopolamine Injection into the Olfactory-Bulb Impairs Short-Term Olfactory Memory in Rats. Behavioral Neuroscience. 1994;108(2):317-24. doi: 10.1037/0735-7044.108.2.317. PubMed PMID: WOS:A1994NJ83000010.

62. Ross JM, Bendahmane M, Fletcher ML. Olfactory Bulb Muscarinic Acetylcholine Type 1 Receptors Are Required for Acquisition of Olfactory Fear Learning. Frontiers in Behavioral Neuroscience. 2019;13. doi: 10.3389/fnbeh.2019.00164. PubMed PMID: WOS:000476971200001.

63. Mandairon N, Ferretti CJ, Stack CM, Rubin DB, Cleland TA, Linster C. Cholinergic modulation in the olfactory bulb influences spontaneous olfactory discrimination in adult rats. European Journal of Neuroscience. 2006;24(11):3234-44. doi: 10.1111/j.1460-9568.2006.05212.x. PubMed PMID: WOS:000243361700027.

64. Martinon D, Lis P, Roman AN, Tornesi P, Applebey SV, Buechner G, et al. Oxytocin receptors in the dorsolateral bed nucleus of the stria terminalis (BNST) bias fear learning toward temporally predictable cued fear. Translational Psychiatry. 2019;9(1):140. doi: 10.1038/s41398-019-0474-x. PubMed PMID: WOS:000466711700001.

65. de la Zerda SH, Netser S, Magalnik H, Briller M, Marzan D, Glatt S, et al. Social recognition in rats and mice requires integration of olfactory, somatosensory and auditory cues. bioRxiv. 2020. doi: 10.1101/2020.05.05.078139.

66. Singer AG, Beauchamp GK, Yamazaki K. Volatile signals of the major histocompatibility complex in male mouse urine. P Natl Acad Sci USA. 1997;94(6):2210-4. doi: 10.1073/pnas.94.6.2210. PubMed PMID: WOS:A1997WP33400024.

67. Yokoi M, Mori K, Nakanishi S. Refinement of Odor Molecule Tuning by Dendrodendritic Synaptic Inhibition in the Olfactory-Bulb. P Natl Acad Sci USA. 1995;92(8):3371-5. doi: 10.1073/pnas.92.8.3371. PubMed PMID: WOS:A1995QR96800062.

68. Cleland TA, Sethupathy P. Non-topographical contrast enhancement in the olfactory bulb. Bmc Neuroscience. 2006;7(1):1-18. doi: 10.1186/1471-2202-7-7. PubMed PMID: WOS:000235339100001.

69. Paxinos G, Watson C. The rat brain in stereotaxic coordinates: compact sixth edition. New York: Academic Press; 2009.

70. Egger V, Svoboda K, Mainen ZF. Mechanisms of Lateral Inhibition in the Olfactory Bulb: Efficiency and Modulation of Spike-Evoked Calcium Influx into Granule Cells. J Neurosci. 2003;23(20):7551-8.

71. Pignatelli A, Belluzzi O. Cholinergic modulation of dopaminergic neurons in the mouse olfactory bulb. Chemical Senses. 2008;33(4):331-8. doi: 10.1093/chemse/bjm091. PubMed PMID: WOS:000255756600003.

72. Saboory E, Gholami M, Zare S, Roshan‐Milani S. The long‐term effects of neonatal morphine administration on the pentylenetetrazol seizure model in rats: The role of hippocampal cholinergic receptors in adulthood. Developmental psychobiology. 2014;56(3):498-509. doi: 10.1002/dev.21117.

73. Rosenthal R, Cooper H, Hedges L. Parametric measures of effect size. The handbook of research synthesis. 1994;621(2):231-44.

Supplemental information

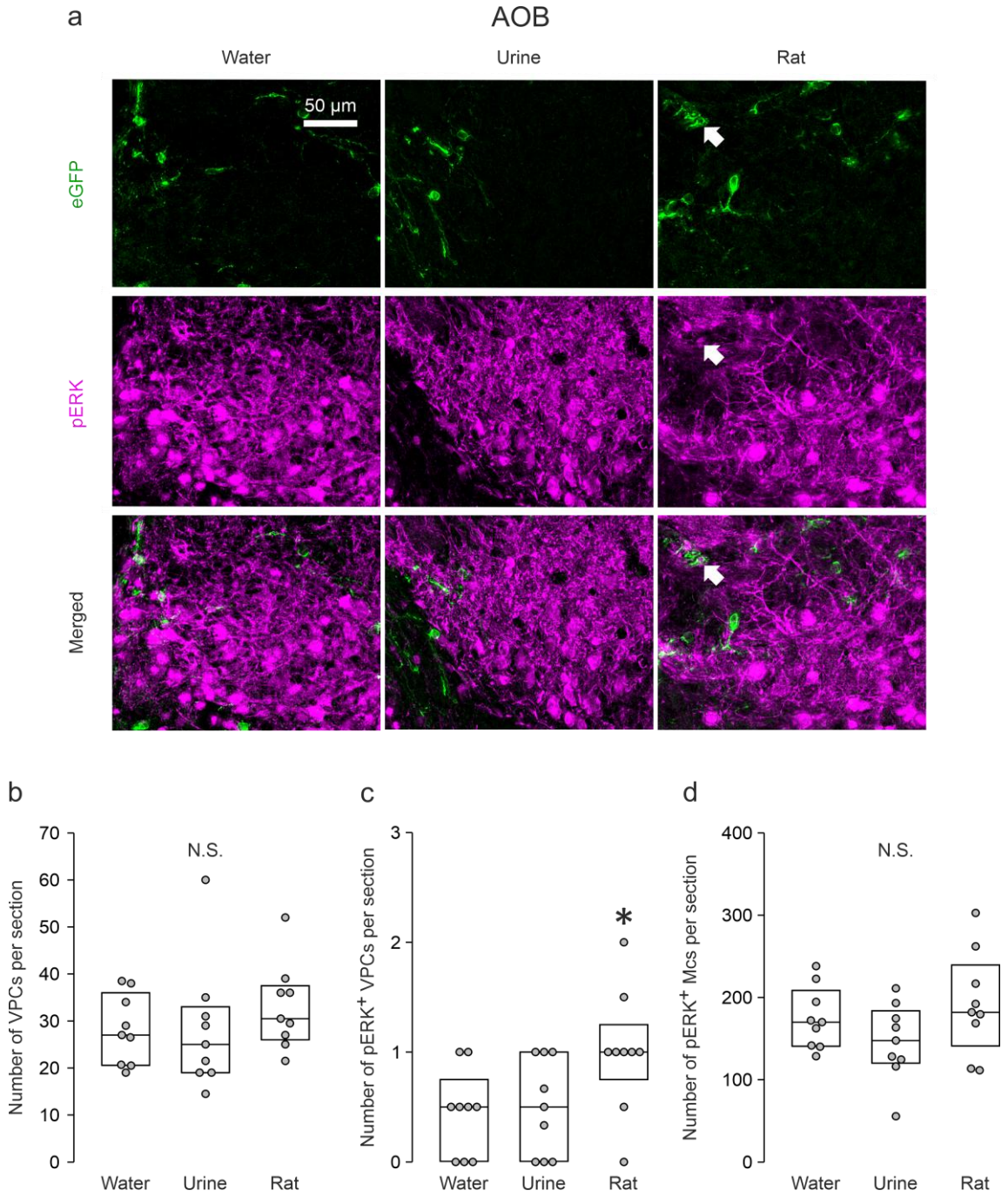

Supplemental Fig. 1 **Social interaction does not activate many AOB VPCs**

(a) Representative average z-projections of the accessory olfactory bulb that were immune-stained for eGFP (green, CF488) and pERK (magenta, CF 594). Arrows indicate a cell that are double-labeled for eGFP and pERK. Scale bar, 50 µm. (b-d) Number of VPCs, of pERK^{+} VPCs or of pERK^{+} MCs per slice in different experimental groups. ANOVA, LSD for single comparison, *p<0.05 vs. Water or Urine, n=9 (water), n=9 (urine), n=9 (rat).

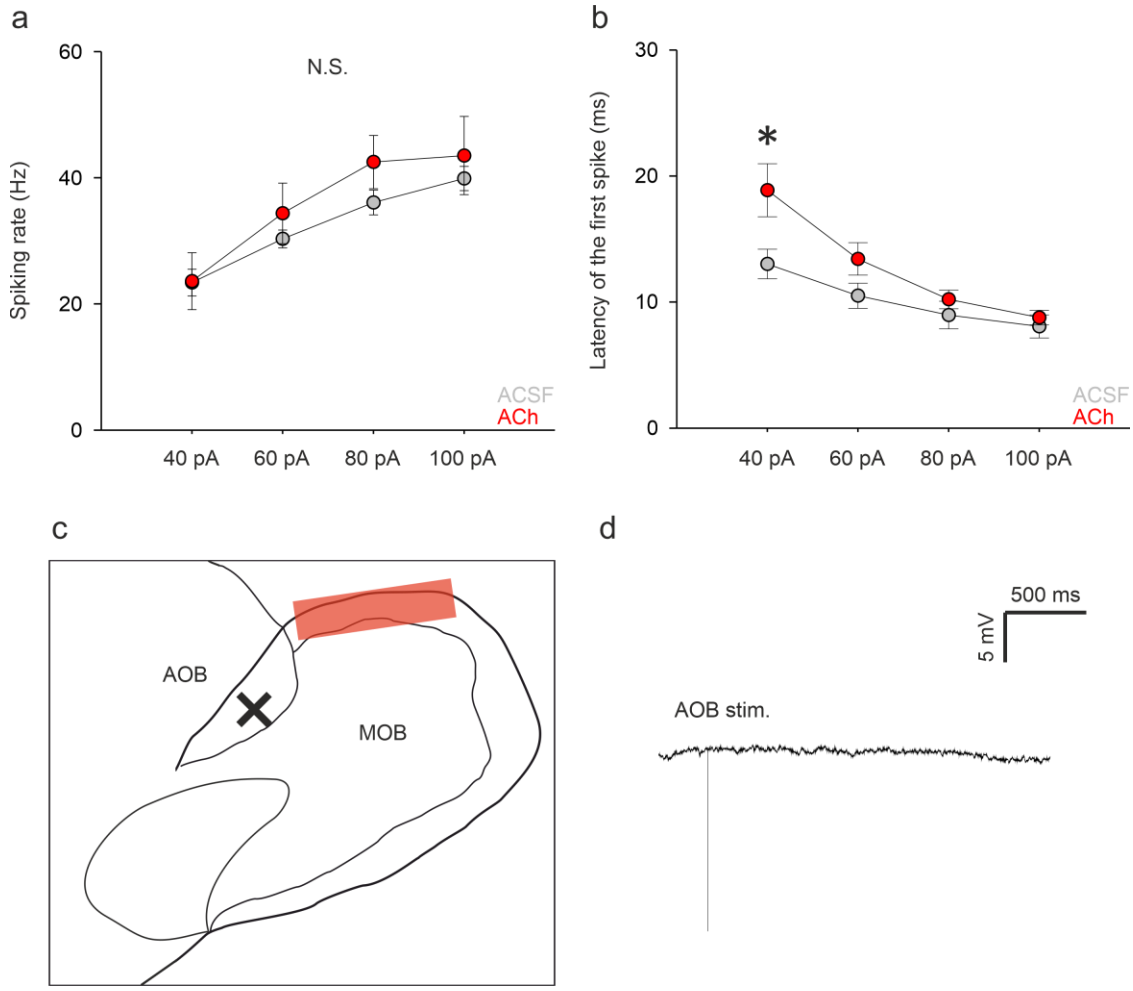

Supplemental Fig. 2 **ACh does not alter intrinsic excitability in VPCs and electrical AOB stimulation does not evoke excitatory responses in MOB VPCs**

(a+b) Spiking rates of action potential trains (left) and latency of the first spike (right) evoked by somatic current injection (40-100 pA) in the ACSF condition (grey) and during bath application of ACh (100 µM, red). (2) × (2) mixed model ANOVA (intensity [within subject] × treatment [within-subject]). N.S., not significant. LSD for single comparison, *p<0.05 ACh (40pA) vs. ACSF (40pA) . Data are means ± SEM. (c) Schematic drawing of the sagittal OB. The cross indicates where the stimulation electrode was positioned. The red bar indicates the dorsal region of the MOB where patch-clamp recordings from MOB VPCs were performed. (d) Representative averaged trace of response from MOB VPCs to electrical vomeronasal nerve/ AOB stimulation (50-500 µA, 100 µs).